Role of Clouds in the Urban Heat Island and Extreme Heat: Houston-Galveston metropolitan area case.

John F. Mejia[1], Juan Jose Henao[2] , Ebrahim Eslami[3]

1. Division of Atmospheric Sciences, Desert Research Institute, Reno, Nevada. https://orcid.org/0000-0001-6727-5541.

2. Escuela Ambiental, Facultad de Ingeniería, Universidad de Antioquia, Medellín, Colombia.

3. Houston Advance Research Center, The Woodlands, Texas. https://orcid.org/0000-0002-7721-6534

Corresponding author: John F. Mejia (john.mejia@dri.edu); 2215 Raggio Parkway, Reno, NV 89512.

Key Points:

- Urbanization correlates with the presence of shallower cumulus clouds.
- Urban clouds are driven by the enhanced sensible heat and dynamic drag imparted by the urban landscape.
- Urbanization cloud enhancement emerges as a crucial pathway responsible for reducing the afternoon Heat Index values.

Abstract

The study and simulation of the Urban Heat Island (UHI) and Heat Index (HI) effects in the Houston-Galveston metropolitan area demand special attention, particularly in considering moist processes aloft. During the warm season, the afternoon sea breeze phenomenon in this coastal city acts as a natural air conditioner for city residents, facilitating the dispersion of pollutants, moisture, and heat. To delve into the intricate relationships among urbanization, clouds, and land-sea interaction, we conducted cloud- and urban-resolving simulations at a 900 m grid resolution. Results show that urbanization correlates with the presence of shallower cumulus clouds, cloud bases at higher altitudes, and increased cloud duration over the Galveston-Houston region compared to rural areas. These urban clouds benefit from the enhanced sensible heat and dynamic drag imparted by the urban landscape, thereby intensifying vertical mixing and moisture flux convergence. This dynamic interplay uplifts heat and moisture convergence, contributing to the enhancement of moist static energy that sustains the additional urban convection. Interestingly, our findings suggest that urbanization augments the mean HI while mitigating its afternoon high. An urban circulation dome emerges, overpowering the influence of land-sea circulations. Contrary to expectations, urbanization doesn't seem to promote a stronger sea breeze that would favor moist and cooler air mass to the city. Instead, the influence of urbanization on cloud enhancement emerges as a crucial pathway responsible for reducing the afternoon HI values. Moreover, uncertainties in SSTs are closely linked to the sensitivities of land-sea circulations, which in turn modulate UHI and extreme heat indicators.

Plain Language

Urbanization influences the meteorology by creating a warmer environment, which enhanced the excessive heat during the summer. Additionally, the warmer environment and the urban buildings increase friction leading more mixing and in turn favoring the development of low-level clouds. We developed computer simulations aiming to understand these processes and further include the role of the sea-breeze in this coastal city. We found that these clouds help ameliorate the excessive heat during the afternoon.

Keywords: Urban clouds, Urban Heat Island, Urban Circulation, Sea Breeze, Heat Index.

1 Introduction

This study is motivated by the need to characterize and better simulate excessive heat in urban environments. Increasing population in urban areas make cities more vulnerable to extreme weather events, climate variations and warming trends. It is likely that some of these changes will be outside of the range of historical extremes (Simolo et al. 2011; Trenberth 2012) and are expected to cause changes not only in mean, but also in extreme weather episodes (USGCRP, 2018). While there is relatively high confidence in the direction of changes in extreme temperature episodes, decision-makers require more quantitative and detail information to make better and more concrete adaptation plans to improve resilience in natural resources management (Rosenzweig et al. 2014) and health related risks (Guo et al. 2018; Ebi et al. 2021). The exposure of cities to extreme heat appears to be more critical under climate change scenarios and is exacerbated by the high solar absorption of the urban environments (i.e., the Urban Heat Island effect, hereafter UHI) (Fischer and Schär 2010; Schubert et al. 2012). High-resolution meteorological models are important tools for both weather forecasts and the development of adaptation and mitigations strategies aiming to make cities more resilient to climate-related risks (Cady et al. 2020; Zonato et al. 2021; Resilient Houston 2020; Houston Climate Action Plan 2020). Hence, understanding the processes modulating the extreme temperature and related uncertainty in the models is a necessary step to add value and gain confidence in forecast products and the climate risk management process.

Recent studies have found that the urban environments not only modulate the temperature via the UHI effect, but also clouds and precipitation (Loughner et al. 2011; Theeuwes et al. 2019; Fan et al. 2020; Doan et al. 2023; Vo et al. 2023). Vo et al. (2023) used long-term satellite clouds retrievals to show that cities enhance clouds. During the daytime, observations (Theeuwes et al. 2019) and numerical simulation (Loughner et al. 2011; Fan et al. 2020; Theeuwes et al. 2021) have shown that the urban environment enhance warm non-precipitating clouds (i.e., low-level shallow cumulus clouds) and even extreme precipitation (Fan et al. 2020; Doan et al. 2023), which we argue can work as a self-cooling mechanism by blocking the incoming solar radiation and increasing evaporative cooling. During the night, however, Vo et al. (2023) suggested that clouds can block outgoing longwave radiation and exacerbate the UHI by suppressing the nighttime cooling. The role of the urban environment on simulated warm non-precipitating low-level clouds needs a more systematic and deeper assessment as it can be influenced by the geography and climate of the region (Theeuwes et al. 2021; Vo et al. 2023; Chiu et al. 2022). Vo et al. (2023) observed, however, that urbanization near Gulf Coast coastal cities tend to show enhanced clouds during the summer. For a single storm event, Fan et al. (2020) simulated the individual and combined effects of the urban land-use/land-cover and aerosols on convective and a storm evolution and intensity. In agreement with Theeuwes et al. (2019, 2021), Fan et al. (2020) showed that Houston urban area is related to earlier occurring and more persistent clouds due to a stronger urban heating and sea-breeze circulation. They also showed that the aerosol-cloud interaction effect can develop deeper convective mixed-phase clouds and more intense storms than the effect of the urban land-use/land-cover alone.

How Houston urban morphology, local circulations, and climate regimes impact the city cloud patterns remain poorly understood. This study focuses on better understanding urban-induced clouds in the Houston area. The local land-ocean sea breeze circulations can invigorate clouds and precipitation (Loughner et al. 2011; Zhong et al. 2017) and overwhelm the signals related to urbanization, dispersion of pollutants (Loughner et al. 2011; Ngan et al. 2013; Caicedo et al. 2019) and aerosol-cloud interaction effect (Fan et al. 2020). Furthermore, Zhong et al.

(2017) showed that under some synoptic conditions, the ACI can overwhelm precipitation processes directly produced by the land-use/land cover and limit the understanding of the interaction between non-precipitation clouds and urban climate. Neglecting aerosol cloud interactions (ACI), we hypothesize that urban-induced clouds can have a significant net surface cooling effect impacting extreme heat indicators.

In this study, we carried out cloud-resolving simulation experiments using the Weather and Research Forecasting (WRF) model coupled with Urban Canopy Modeling focused over the Houston-Galveston area to assess the impact of non-precipitation clouds on the extreme heat indicators during the modeling period. Moreover, we assess some model uncertainties by contrasting cloud and extreme heat indicators sensitivities to low-level moisture fluxes related to sea surface temperature biases.

2 Data and Methodology

2.1 The regional climate model coupled with the Urban Canopy Model

We used the Weather Research and Forecasting model (WRFv4.3.2; Skamarock et al. 2008) coupled with the Urban Canopy Model (UCM) to perform urban- and cloud-resolving simulations for 1-16 August 2020 . We implemented the UCM based on the multi-layer building effect parameterization (BEP) scheme coupled with the Building Energy Model (BEM; Salamanca et al. 2010). This UCM option considers three-dimensional mass and momentum mixing and heat transfer between buildings and provides a realistic and accurate representation of near-surface energy fluxes and air temperature in mid-latitude cities (Cady et al. 2020; Jin et al. 2021). We would like to stress that this is not an instance of model calibration, but an attempt to assess and understand the UCM's capabilities and related uncertainties. We used this UCM option, among others available, because it incorporates 11 Local Climate Zones (LCZ), and it can be coupled with a solar photovoltaic-panel and green roof parameterization schemes (Zonato et al. 2021) that will be implemented in an urban heat mitigation assessment.

We acknowledge that it is difficult to find a model configuration that is superior under different flow regimes and the large variety of geography and urbanization settings. In this study, we used a three nested domain configuration (8100 m, 2700 m, and 900 m) centered in Houston, with 61 vertical levels up to 100 hPa. To allow the innermost model domain to relax towards the scenario settings, we designed the borders to be at least 80 km away from the suburban areas of Houston. Our initial modeling tests showed significant numerical diffusion noise highlighted as non-physical wind street patterns and thermal fields in the mixing layer with a spatial scale of two times the grid size. This problem is relatively common in high-resolution simulations during weak wind conditions and weak or unstable stratification (Knievel et al. 2007; Crosman et al. 2012). We imposed a spatial filter based on an explicit 6th-order numerical diffusion scheme with a non-dimensional rate of 0.12. Despite the potential over smoothing of surface processes, the explicit diffusion treatment notably improved simulations, and results were resistant and unsensitive to its implementation. Additionally, we combined our experience and literature reports to determine other configurations and selection of physical parameterizations implemented in our model. For parameterization of moist processes, we used the Thompson double-moment microphysics, whereas convection and clouds parameterization are resolved explicitly in all our model domains, except for the coarser grid (8100 m) where we used the Kain–Fritsch scheme. Additionally, we used the Dudhia and RRTM as shortwave and longwave radiation schemes, respectively; Noah-MP, Monin-Obukhov and YSU as land-surface model, surface layer, and planetary boundary layer

(PBL) schemes, respectively. YSU PBL scheme was used for its simplicity, low computational cost and recognized good performance (Hendricks et al. 2020). The first 6 hours of simulations were not considered to allow for the model spin up. We used the NCEP GDAS/FNL 0.25 Degree Global Tropospheric Analyses and Forecast Grids (hereafter "FNL") as initial and boundary conditions data, with SST skin temperature updated as bottom boundary condition SSTs every 6 hours.

2.2 Land Use/Land Cover and Urban Characterization

An important consideration in urban canopy modeling is the characterization of the Land Use/Land Cover (LULC) and urban categories. Most LULC products rely on remote sensing surveys with urban classification that are either outdated, such as the National Urban Database and Portal Tool (NUDAPT - 2009) or lack details even in major urban composition features, such as the World Urban Database and Access Portal Tools version 2 (WUDAPT - 2016; Brousse et al. 2016; Ching et al. 2018; Demuzere et al. 2021, 2022). Additionally, differences in the algorithms used to characterize urban categories and different data sources may result in different urban coverage. We opted to implement the 100 m global WUDAPT data (Demuzere et al. 2022) for the following considerations, including: WUDAPT (2016-2018) data is more modern than NUDAPT (2006) and captures a more recent snapshot of the urban growth with better resolution; and LCZ adaptation to WUDAPT favors the implementation of the UCM BEM+BEP for 11 different urban categories, contrasting only three urban categories in the NUDAPT data.

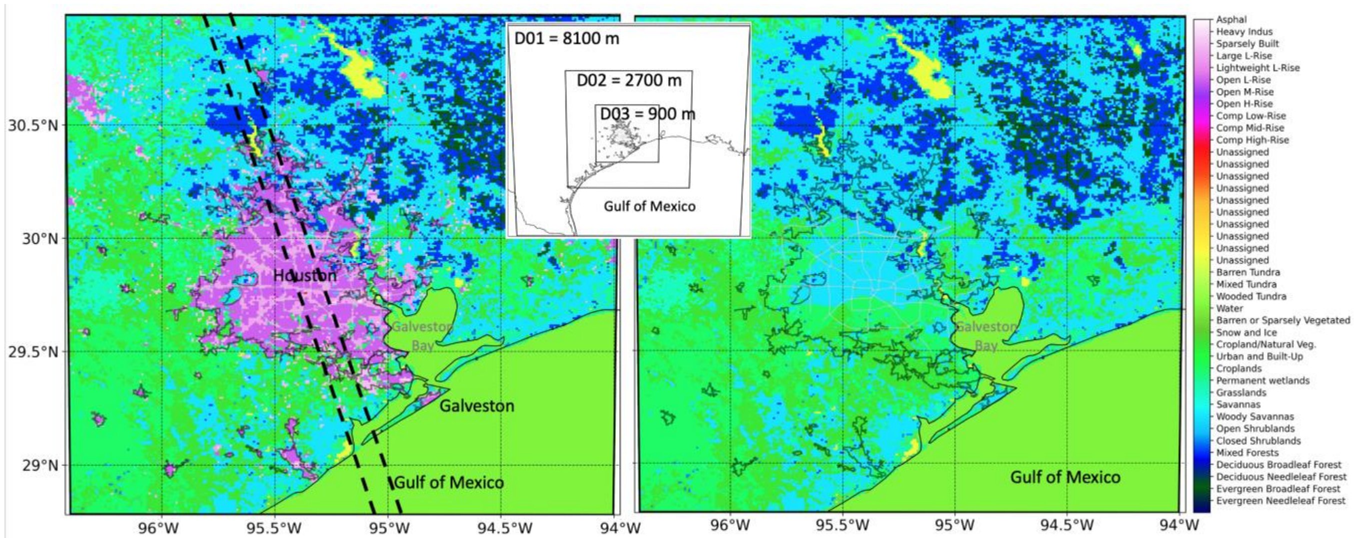

Figure 1. (left panel) Model inner domain (900 m) Land Use/Land Cover (LULC) based on WUDAPTv2 using Local Climate Zones for the urban areas and MODIS for rural areas; dash lines show the location of the cross-city transect shown in the analysis. (right panel) LULC after removing the urban areas and replacing them with surrounding predominant rural vegetation. Inset shows the nested domain configuration. Dark grey contours indicate urbanization boundaries as of 2010 (Houston-Galveston Area Council, H-GAC; https://www.h-gac.com/Home) and light grey show location of major intraurban highways. Fore reference, inset in the middle shows all model domains.

2.3 Surface Station and Upper-air Winds

We used all available, reliable, quality-controlled surface station regular monitoring sites in the Houston area and surrounding rural land. Information was downloaded via the MesoWest portal (https://mesowest.utah.edu/) but provided by the National Weather Service, Remote Automated Weather Station, and Texas Commission on Environmental Quality (TCEQ) Continuous Ambient Monitoring Station (CAMS) network. A total of 150 stations passed our quality assurance/quality control filters (e.g., less than 5% of missing data after removing outliers, visual inspection, atypical diurnal cycle of temperature and relative humidity) with 117 sites located in urban (112 in Open L-Rise; 4 in Large L-Rise; and 1 in Open H-Rise) and 31 in rural land use/land cover categories. These surface observation data helped further constrain the model in its diurnal evolution behavior in temperature, relative humidity, and winds, while augmenting the information to examine derived parameters such as: low temperature (Tmin); high temperature (Tmax); Urban Heat Island (UHI) effect, estimated as the difference between representative urban minus rural sites; and Heat Index, following Rothfusz (1990) formulation. We acknowledge the potential of siting uncertainties in the urban networks and sensors (117 sites), some of which are designed for air quality monitoring purposes (e.g., TCEQ sites). We assessed the confidence in the model by estimating the model bias, root-mean-square-error (RMSE) and Pearson correlation coefficient statistics. To partly address the uncertainties related to the relatively short simulations (e.g., dominance of any synoptic settings) and the potential effect of diurnal mesoscale constrains or geographical heterogeneities (e.g., sea-land circulations, distance from the coast and Galveston bay), we performed a bootstrapping with replacement approach any time it was possible.

To evaluate the performance of the simulated low-level winds, we used the Cooperative Agency Profilers wind profiler observations at La Porte (LPTTX; Cooperative Agency Profilers https://madis-data.noaa.gov/cap/), located near the coast at the northern shores of Galveston Bay. When the model is contrasted against the observations, we excluded the initial 6 hours due to model spin-up issues. To isolate the effect of the intermittent and scattered summer showers, we constrained the error analysis to days without significant observed precipitation events (< 5 mm) in the Houston-Galveston area; showers were mostly concentrated during Aug 1-3 (not shown).

2.4 Model Experiment Design

2.4.1 SST Sensitivity

The city's proximity to the Gulf of Mexico and the complex coastal shape of Galveston Bay warrants a careful look at the SST data used by the model as bottom boundary conditions (Hawbecker and Knievel 2022). An effort to improve the simulated thermal gradients will be the careful implementation of the remotely sensed NOAA-SNPP VIIRS SST dataset (available daily at 4 km grid size; several snapshots per day; Bouali and Ignatov 2014). We carried simulations using the SST fields as they are provided by the FNL bottom boundary conditions (hereafter 'biased' SSTs). From these untreated SSTs, we performed a time-space bias correction using the remotely sensed and buoys data. When comparing measurements from these platforms and default fields used by the model, we found an average offshore FNL SST cold bias of nearly -1°C (SFig. 1). We implemented a Barnes interpolation approach with successive correction using a Gaussian weight function departing from the background field (the biased SSTs) until optimizing the agreement between the interpolated function and the measurements (the unbiased SSTs).

2.4.2 Clouds, Urbanization and Weather Sensitivity

To isolate the intricate role of the synoptic effect, sea-breeze, and cloud effects from that of the urbanization effect, we performed several simulations. The influence of moist processes (clouds and precipitation) is important in characterizing the temperature and relative humidity in Houston. Cloudy afternoon and showers forced by the sea-breeze can make a significant difference in the UHI environment (Morris et al. 2001). However, due to the relatively short simulations (15 days) and the intermittent nature of the moist processes (clouds and precipitation), we performed a set of simulations that isolate the influence of clouds and showers in the area. Simulations without clouds helped us produce an upper boundary in surface radiation conditions but mesoscale dynamical changes in relation to the clear sky environment are still expected. Additionally, during the simulation period, different meteorological regimes could have modulated sea-breeze related convection invigoration: 1-3 Aug a pre-trough regime, 4-5 Aug a post-trough regime and 5-16 Aug the Bermuda high anticyclone was more pronounced

(Want et al. 2022; https://earth.nullschool.net/). Hence, we developed a clear sky simulation (e.g., fully turning off microphysics and convection) to help analyze the results. Hence, simulations with (Baseline) and without (hereafter 'Clear sky') clouds and precipitation were performed and combined with model realizations similar to Baseline but perturbing the offshore bottom boundary conditions using bias corrected SSTs fields (hereafter 'Biased SSTs) or removing all urban areas in the domain (hereafter 'No City'). Table 1 shows a summary of the simulations that were performed in this study, as well as their related description and justification. All references to the model simulation are related to the All sky-Baseline scenario (hereafter 'Baseline'), unless otherwise stated.

Table 1. Description of model scenarios simulated in for this study.

Scenario name	***Description***	***Justification***
Baseline	*Baseline with simulation of cloud and convective processes (moist processes) and bias correction of offshore SSTs*	*Full physics simulation using outlined parameterizations and state-of-the-art LULC categories from LCZ. Systematic biases associated with offshore SSTs are removed.*
Clear Sky	*Same as Baseline but without clouds and moist convective processes.*	*Isolate the role of clouds and precipitation relative to Baseline.*
Biased SST	*Same as Baseline but with biased offshore SSTs*	*Assess the sensitivity of Baseline to SST perturbations or refinements (e.g., bias corrections).*
No City	*Same as Baseline but removing the urban LCZ categories and replacing them for representative vegetation in the region.*	*Isolate the role of the urbanization in the meteorology.*

3 Results

3.1 Model Evaluation

Figure 2 shows the observed and simulated diurnal patterns of surface temperature, relative humidity, Heat Index, and zonal and meridional winds, corresponding to urban and rural sites in the domain. In general, the model adequately follows the diurnal median patterns for all the evaluated parameters, but several biases are apparent with the model showing a systematic dry bias (also exhibited in the water vapor mixing ratio, not shown) that is more intense during the afternoon and nighttime. The model surface temperature shows an in-phase diurnal evolution with a warm bias in the late afternoon and during the nighttime. Of note is that model nighttime temperatures biases are even warmer in urban sites compared to rural sites. Intercomparison between the urban and rural sites is only possible because we performed a bootstrapping approach with replacement to assess the uncertainty of the results with respect to the distance from the coast and its land-sea interaction effects. Relative to Houston, the stations included contained nearly equal number of sites closer to the coast and further inland.

To evaluate the model performance of the low-levels (< 3 km) circulation, we used surface stations and La Porte wind profiler observations. Fig. 2 shows that the diurnal distribution of the simulated zonal winds closely follows the observations, with shifting from relatively calm southeasterlies in the morning to stronger southwesterlies in the afternoon and nighttime. Part of the wind shifting feature is typically a result from the planetary boundary layer diurnal inertial oscillation (Blackadar 1957); diurnal variability at this region can also be driven by the land-sea circulation. A striking surface circulation feature is that wind speeds are stronger over rural areas compared to urban areas (Fig. 2). This urban-rural wind speed differences are overemphasized by the model: the simulated winds show a slightly stronger southerly wind bias in urban sites, whereas it almost doubles the observed southerly wind in rural sites. Fig. 3 shows low-level winds at La Porte, highlighting an observed peak at midnight and between 250-500 m above the ground, whereas the model shows a deeper maximum at 01-02 LT and centered between 300-400 m above the ground. In agreement with the evolution of the surface diurnal pattern, the model overemphasizes the low-level winds and shows an earlier (15 compared to 12 LT) southwesterly wind increase in the afternoon. During the evening and nighttime, the low-level flow further accelerates until early in the morning. This nocturnal acceleration is connected to the prevailing summertime Great Plains Low-level Jet circulation that extends to the Gulf coast in eastern Texas (Pu and Dickinson 2014). Early in the morning, the land breeze and vertical mixing decelerates the nocturnal jet. In intensity, this nocturnal jet shadows the diurnal variability related to the local land-sea breezes. Ngan et al. (2013) showed similar model biases patterns and intensities irrespective of different land surface and PBL parameterizations.

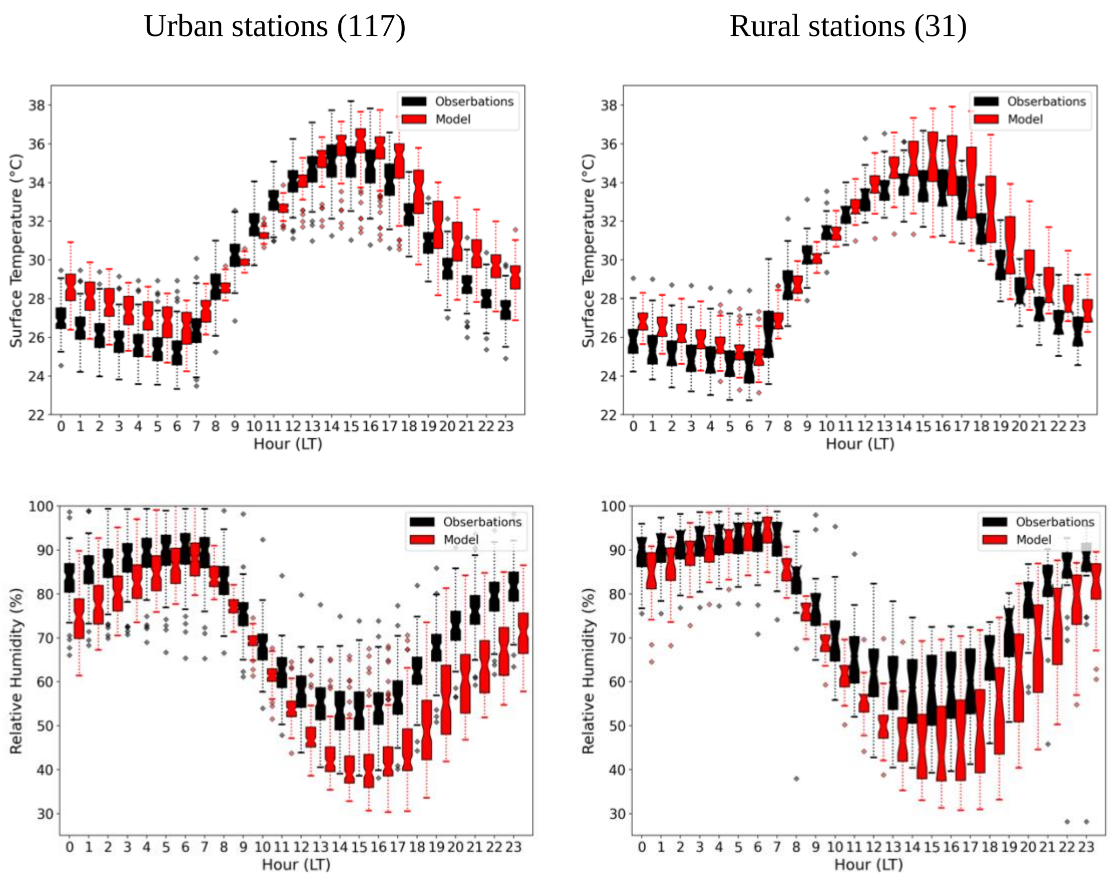

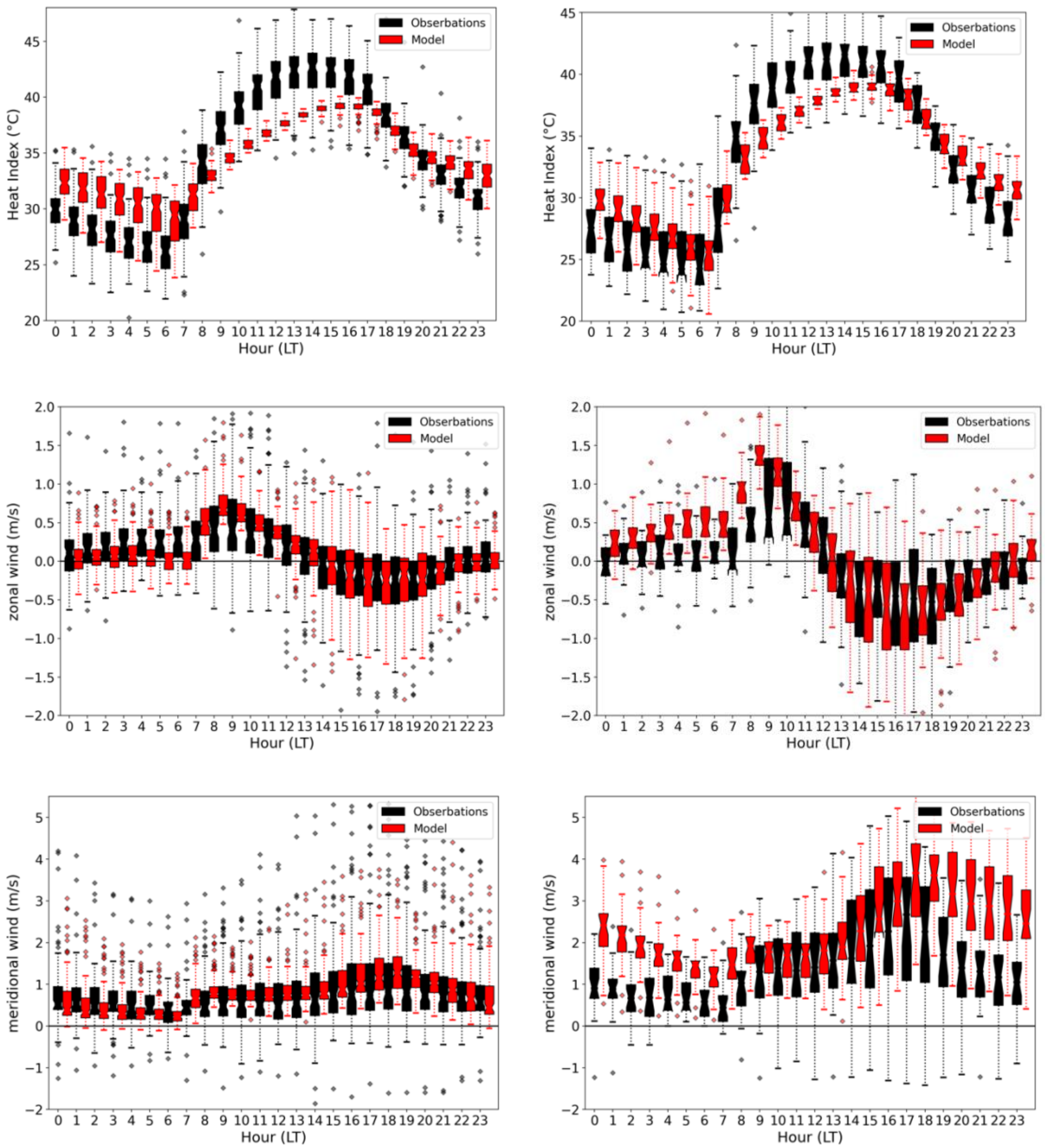

Figure 2. Baseline model and observed diurnal cycle distribution of (top to bottom panels) surface temperature, relative humidity, and zonal and meriodonal wind components for stations in the Houston urban (115 sites; left panels) and rural regions (31 sites; righ panels).

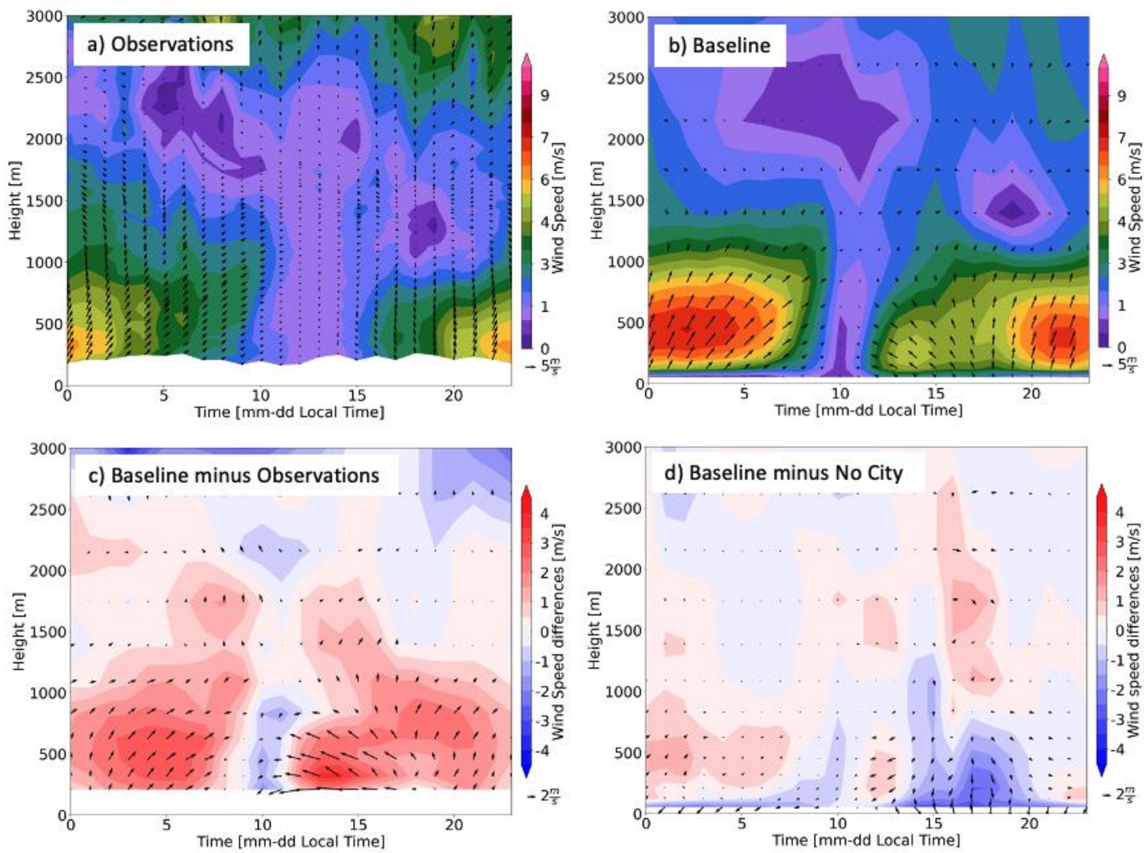

Figure 3. Low-level-diurnal mean horizontal wind speed (contours) and wind vectors (with the north direction pointing upwards) for (a) La Porte Wind profiler observations, (b) Baseline model winds, (c) Baseline minus observations differences and (d) Baseline minus No City differences.

Figure 4 shows the observed and all simulated model scenarios (Table 1) and simulation biases evaluated at all available surface station sites (see SFig. 2 for evaluation of the RMSE and Pearson correlation coefficients). In general, model errors are small and well within the model typical behavior in perturbed sensitivity experiments (Ancell et al. 2018; Wang et al. 2023), but some systematic error signals emerged as a function of the scenario simulations and by compositing rural and urban areas. Over both urban and rural areas, the Baseline simulation shows a systematic warm bias for Tmin and Tmax. Not surprisingly, over the urban areas the No City scenario shows a relatively colder bias when compared to all the urbanized scenarios. The role of clouds in the model performance is apparent. Notably, during the daytime the biases are warmer (and drier) for the Clear sky scenario, as the lack of clouds increases the incoming solar radiation, balanced by more sensible and ground heating. At night, the warmer biases of the Clear sky scenario relative to Baseline biases suggest that the outflux ground heating dominate the faster longwave radiation cooling (Fig. 5). When comparing the Baseline to the Biased SSTs scenario, refining the offshore SSTs towards a warmer SSTs have a significant warming effect, with larger differences during early morning. Therein, a surprising result is that bias differences between Baseline and Biased SSTs during the daytime are smaller than those during early morning; the direct sea-breeze advection of warmer maritime surface temperature during the daytime does not develop significant sensitivity in Tmax in comparison to Tmin. Therefore, the model biases highlight that the surface temperature sensitivity between the Baseline and Clear sky simulations (-0.56 °C difference) are significantly larger than that between the Baseline and Biased simulations (0.25 °C difference; see also SFig. 2). By construction, the bias trends in this model evaluation procedure are somehow expected, but some potential non-linear impacts related to changes in cloudiness and circulation, which motivates the main objective of this study, are not as apparent.

a) Surface temperate

b) Relative humidity

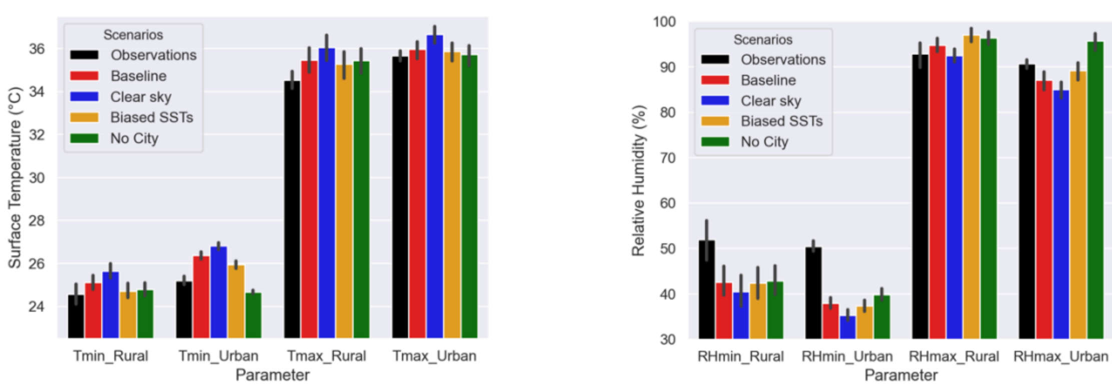

c) Surface temperature bias

d) Relative humidity bias

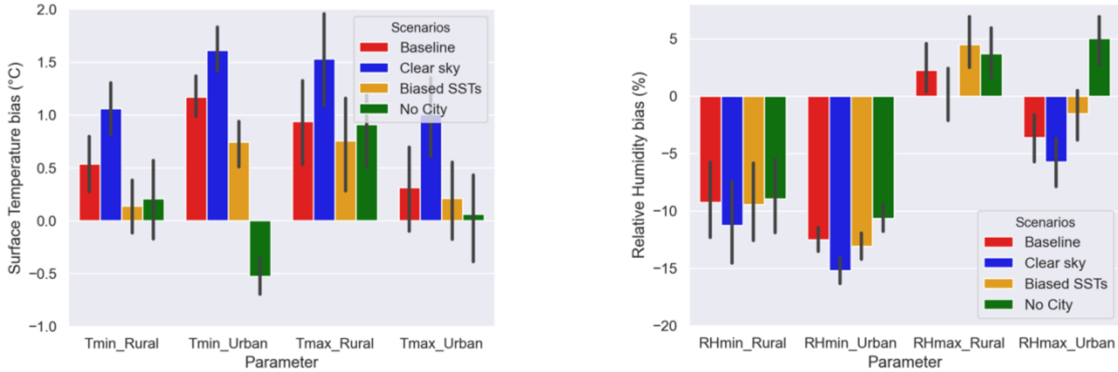

Figure 4. Observed and different model scenarios (Table 1) evaluated at surface station sites for low and high (a) surface temperature and (b) relative humidity, and corresponding (c, d) bias distribution. Surface station sites are categorized as Urban or Rural according to MODIS/WUDAPTv2 land use/land cover types. Evaluation period is 1-16 August 2020. Analysis constrained to non-rainy periods as described in the text.

a) Sensible heat flux

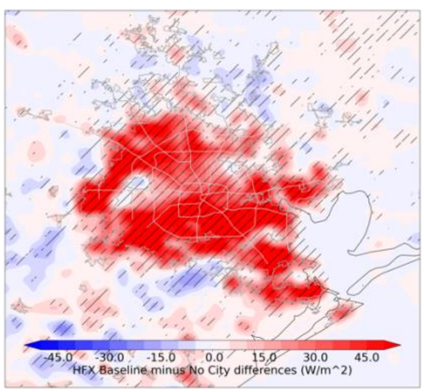

b) Sensible heat flux

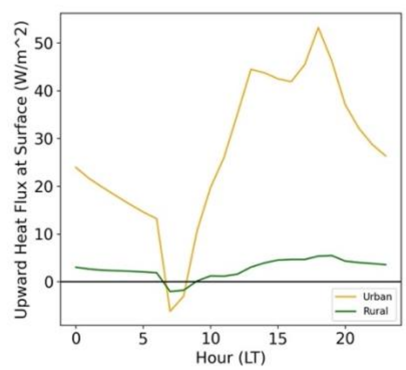

c) Latent heat flux

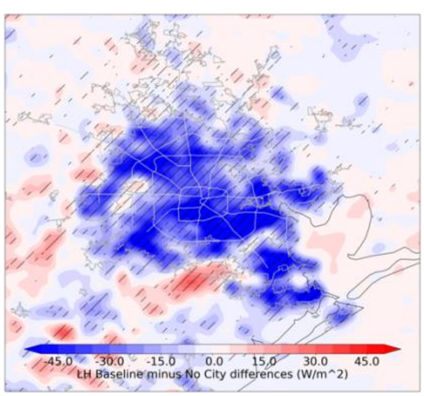

d) Latent heat flux

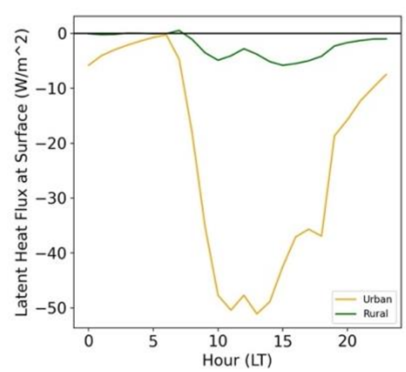

e) Ground heat flux

f) Ground heat flux

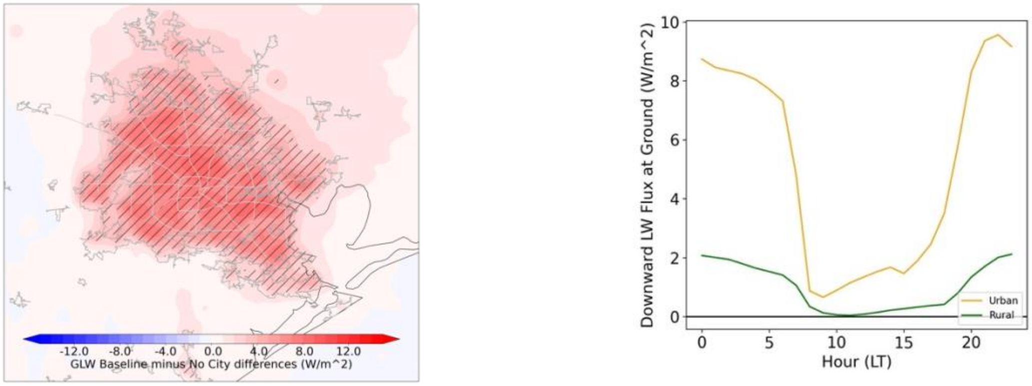

Figure 5. Mean Baseline minus No City differences for (a) sensible, (c) latent, (e) ground heat fluxes. Hatched areas indicate that differences are significant with a 95% confidence level. Dark grey contours indicate urbanization boundaries as of 2010 (Houston-Galveston Area Council, H-GAC; https://www.h-gac.com/Home) and light grey show location of major intraurban highways. Spatially averaged diurnal (b) sensible, (d) latent and (f) ground heat fluxes for Baseline minus No City differences composited by urban and rural areas.

3.2 Urban Heat Island

Table 2 compares surface station observations and corresponding simulations composited as a function of the rural and urban categories. The UHI was estimated as the mean of the mean of the stations in the urban minus rural sites. Since the distance from the coast (i.e., from the station to the nearest simulated ocean grid point) can have an impact in the UHI estimates, we balanced the number of sites located near the coast with those far from the coast. Observations show a more pronounced UHI effect during the Tmax times than during the Tmin times. When contrasting the model at sites with surface station data, the Baseline model is overemphasizing nighttime and early morning UHI effect and underemphasizing that of the afternoon; herein, no effort was made to examine and evaluate the timing of the Tmin and Tmax. Earlier, however, we showed that the mean cycle of temperature in the model is in-phase with the observations (Fig. 2). Table 2 also shows that the Baseline simulation is related to a stronger early morning and milder afternoon UHI than the Clear sky scenario. This is not surprising due to the role of clouds in the long and short wave radiative balance (Brenguier et al. 2000). Biased SST simulation yields a similar and more intense early morning and afternoon UHI, respectively. Finally, the relatively small UHI effect based on the No City simulation shows that the composited UHI are linked to urbanization.

Another method to reveal the intensity of the UHI is by comparing the Baseline and the No City scenarios. Fig. 6 shows the UHI effect spatial patterns during Tmin and Tmax times as estimated by the Baseline minus the No City simulated differences. The nighttime and daytime UHI differences are striking, highlighting a very pronounced and significant early morning UHI effect and a less intense afternoon UHI effect (Fig. 6c). The urbanization intensity and intra-urban vegetation islands are related to some of the cool UHI patches within the city (Fig. 1); albeit that differences can also be a function of the distribution of the underlying vegetation assigned in the No City scenario instead of the urbanized LCZ. Notably, the Baseline minus the No City differences remain significant downwind and to the north and northwest of the city boundary (Fig. 3). Since some stations are located downwind of Houston, this advection of UHI can reduce the actual UHI intensity estimates shown in Table 2. Hence, the overemphasis of the early morning UHI can be partly attributed to the overestimation of surface temperature in the urban areas.

Table 2. Observed and simulated mean Tmin and Tmax at surface station locations composited by rural (31 sites) and urban (115 sites) locations. Urban Heat Island effect is estimated as the urban minus rural difference. Urban and rural categories are assigned following MODIS/WUDAPT and LCZ designation in the model.

	Rural	Urban	Rural	Urban	UHI (Urban minus Rural)	
	Tmin [°C]		Tmax [°C]		Tmin [°C difference]	Tmax [°C difference]
Observations	24.56	25.18	34.52	35.65	0.62	1.13
Baseline	25.10	26.35	35.46	35.96	1.25	0.50
Clear sky	25.62	26.80	36.05	36.65	1.18	0.60
Biased SSTs	24.70	25.93	35.28	35.86	1.23	0.58
No City	24.77	24.66	35.43	35.71	-0.11	0.28

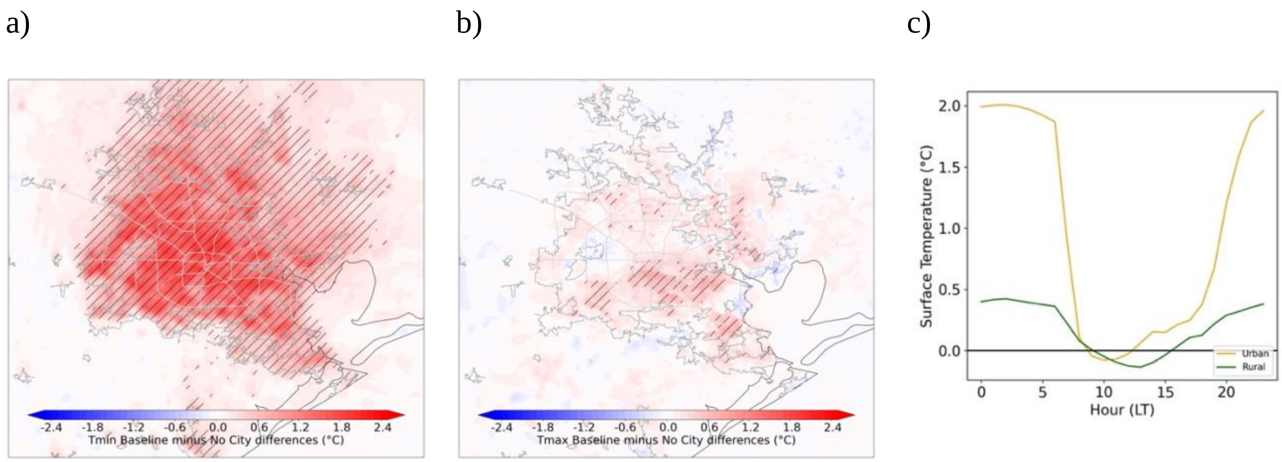

Figure 6. Mean Baseline minus No City differences for (a) Tmin and (b) Tmax. Hatched areas in (a) and (b) indicate that differences are significant with a 95% confidence level. Dark grey contours indicate urbanization boundaries as of 2010 (Houston-Galveston Area Council, H-GAC; https://www.h-gac.com/Home) and light grey show location of major intraurban highways. (c) Spatially averaged diurnal surface temperature for Baseline minus No City differences composited by urban and rural areas.

3.3 The Role of Shallow Cumulus Clouds

Figures. 7a and 7b show the mean vertical maximum cloud mixing ratio for the Baseline and No City scenarios, respectively. The Baseline urbanized area exhibits thicker and more abundant clouds compared to the urban area in the No City scenario, primarily attributed to afternoon shallow cumulus clouds (Fig. 7c). In contrast, the No City scenario shows less abundant cloud cover with less apparent differences across the domain. The impact of urbanization in the cloud patterns is complex and can vary temporally and spatially. It is important to note that the patchy cloud structures are a result of the relatively short simulation, limiting a point-by-point comparison between these scenarios. However, extending the model integration over a longer duration is expected to reveal more robust and discernable differences. For instance, the cloud frequency climatology by Wilson and Jetz (2016) unambiguously demonstrates that urbanization-related clouds are more frequent than clouds in the surrounding rural areas. This cloud climatology, developed at a 1 km grid size, further reveals intraurban variability in cloud frequency dependent on urbanization intensity and urban green infrastructures, as observed in the less cloudy areas over the vegetated Addicks and Barker flood control reservoirs in the west of Houston (Fig. 1).

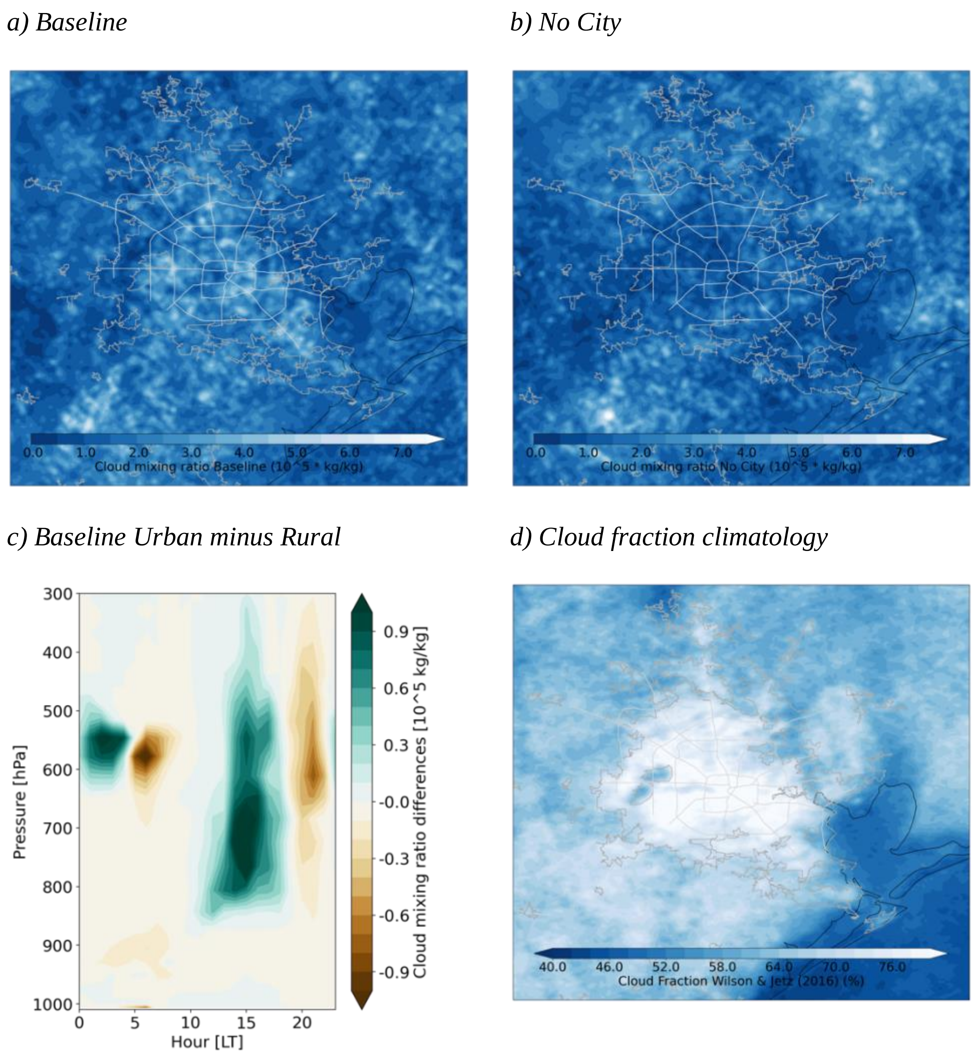

Figure 7. Mean vertical maximum cloud mixing ratio for (a) Baseline and (b) No City scenarios, and (c) Baseline diurnal-pressure urban minus rural composites. (c) Wilson and Jetz (2016) cloud fraction climatology based on 15 years of twice-daily Moderate Resolution Imaging Spectroradiometer (MODIS) satellite images. Dark grey contours indicate urbanization boundaries as of 2010 (Houston-Galveston Area Council, H-GAC; https://www.h-gac.com/Home) and light grey show location of major intraurban highways.

The impact of urbanization in the clouds is more apparent by averaging their properties in space. Fig 8 presents the spatially averaged diurnal-pressure cloud mixing ratio for both the Baseline and the No City scenarios. In general, inland shallow cumulus clouds begin forming early during the daytime, growing deeper and more abundant around 15 LT. The Baseline simulation shows that these clouds are more abundant in the urban areas than in the rural areas, while Baseline minus No City differences further confirm that over the urban areas these shallow cumuli are more abundant, grow deeper and last longer. Although smaller differences are observed when comparing clouds between the Baseline and No City scenarios in rural areas, some cloud mixing ratio differences are simulated, likely due to the advection of UHI effects downstream into rural regions (Fig. 6). Other contributing factors may include changes in mesoscale land-sea circulation, evident from offshore cloud mixing ratio differences (Fig 8), or potential numerical noise effects.

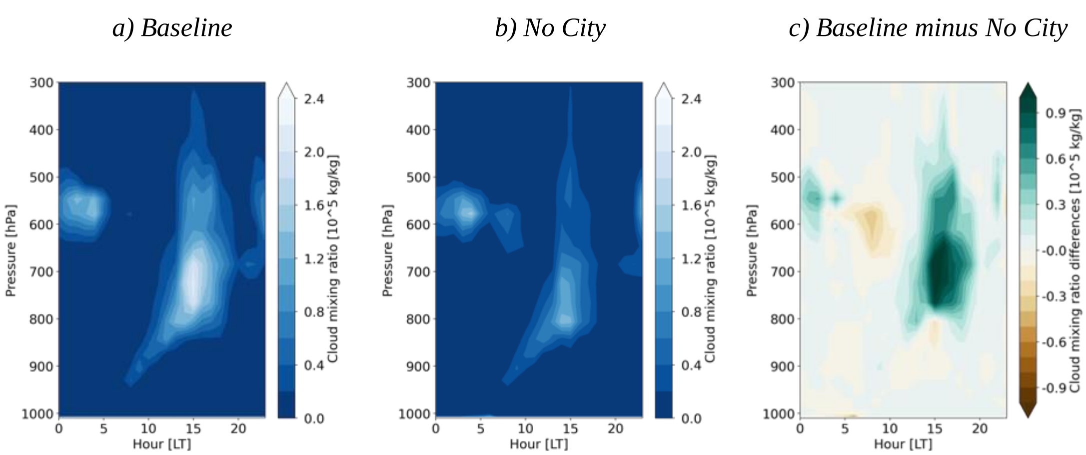

Figure 8. Diurnal-pressure mean cloud mixing ratio for a) Baseline, b) No City and c) Baseline minus No City scenarios spatially averaged over urban categories according to MODIS/WUDAPTv2 land use/land cover types.

Figure 9 shows that the cloud base is significantly higher and thicker in the urban mixing layer dome. Compared to the rural areas, an increase in cloud base height is expected in environments with lower relative humidity (Williams et al. 2015) or higher Bowen ratio (Chiu et al. 2022). Additionally, it is possible that the thicker mixed layer is favored by enhanced sensible heat flux (Fig. 5) and by the increased urban aerodynamic roughness exhibited as a flow slowdown over the urban area (Fig. 3). The low-level flow deceleration of the predominant south-southeasterly wind, as it flows over the urban area, is apparent in Fig. 10. Notably, the urban PBL diurnal differences are damped around the time of maximum shallow cumulus (~15 LT), in which the enhanced clouds control a transient surface cooling effect, hence temporarily reducing the vertical mixing.

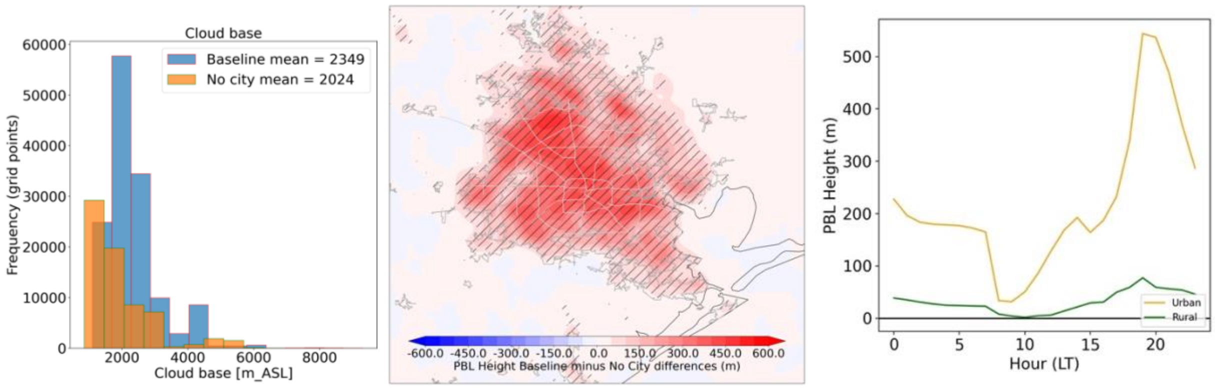

Figure 9. (Left panel) Cloud base distribution for Baseline and No City scenarios as occurring over the urbanized area. Student's t-test and Kolmogorov–Smirnov test indicate that means and distributions are significantly different with 99% confidence level. (Middle panel) Baseline minus No City PBL height differences with hatched areas indicating that differences are significant with a 95% confidence level; Dark grey contours indicate urbanization boundaries as of 2010 (Houston-Galveston Area Council, H-GAC; https://www.h-gac.com/Home) and light grey show location of major intraurban highways. (Right panel) Baseline minus No City PBL height differences averaged over urban and rural areas.

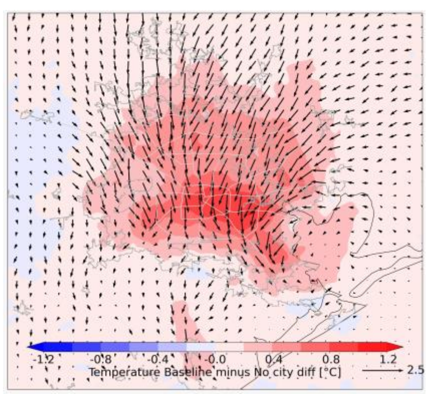

Figure 10. 500 m ASL temperature and wind vectors for Baseline minus No City differences averaged between noon and 18 LTC. Dark grey contours indicate urbanization boundaries as of 2010 (Houston-Galveston Area Council, H-GAC; https://www.h-gac.com/Home) and light grey show location of major intraurban highways.). Wind vectors are plotted only every 6 grid points to avoid cluttering.

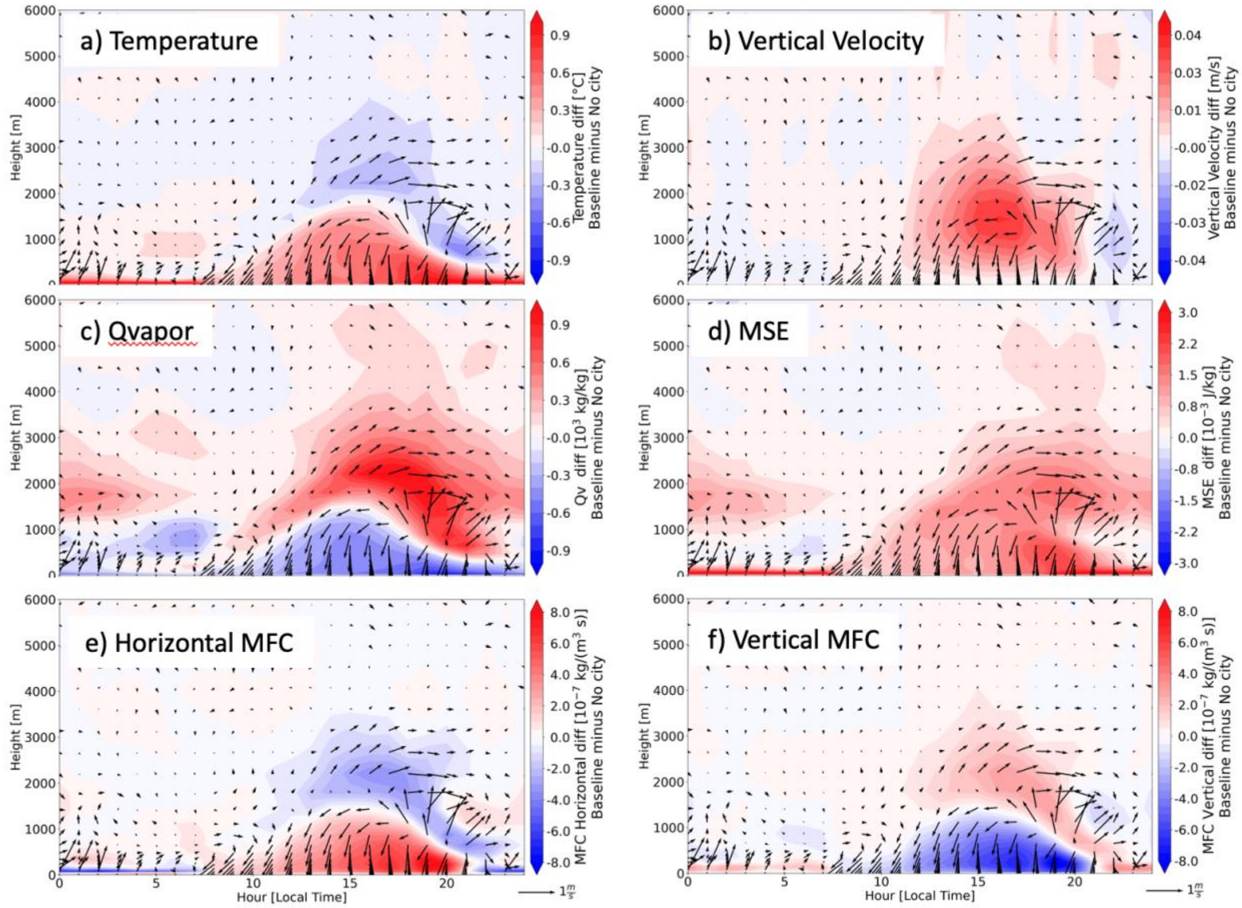

Figure 11. Diurnal-height Baseline minus No City scencario differences spatially averaged over the urban areas for (a) temperature, (b) vertical wind component, (c) water vapor mixing ratio, (d) moist static energy (MSE), (e), horizontal moisture flux convergence, and (f) vertical moisture flux convergence. Vectors in each panel correspond to the horizontal wind, with the north direction pointing upwards. In the vertical, wind vectors are plotted only every 6 grid points to avoid cluttering.

To better understand the factors driving enhanced clouds over the urban dome, we examined the diurnal-height urbanization impacts for various dynamical and thermodyncamical parameters (Fig. 11). Synchronous with enhanced afternoon uplift, the urban dome extends higher with a dipole of warmer and drier airmass over the city and cooler and moister air mass in the upper-mixing layer. A significant feature in Fig. 11 is that the mixed layer air entering the clouds is related to enhanced Moist Static Energy (MSE), likely supported by the increased sensible heat and warmer temperature near the surface, as well as enhanced moisture in the upper-mixed layer. Dynamically, this air mass is sustained by the enhancement of both horizontal moisture flux convergence at low-levels and upward moisture flux convergence in the upper-mixed layer. Additionally, an urban-induced circulation cell with northerly low-level and south-southwesterly upper-mixed layer circulation disturbance (and enhanced moisture flux divergence) is apparent. This circulation pattern in the urban dome resembles the self-contained UHI circulation described by Fan et al. (2017). Moreover, Fig. 10 clearly highlights the horizontal extent of the low-level branch of this circulation, impacting beyond the urban area and well downstream of the city.

It is possible that shallow cumuli and enhanced precipitation (not shown) moisten the cloud and subcloud layers, further favoring more cloud development. Fig. 12 displays a bulk mixing line analysis with the thermodynamical structure of conserved variables (potential temperature and water vapor mixing ratio) in the subcloud layer. The enhanced frequency in the Baseline entrainment and downdrafts zones further suggests a more active cloud dynamics. Notably, when compared to the No City simulation, the Baseline simulation shows that surface fluxes predominantly provide a warmer and dryer mixing lines, with enhanced downdrafts moistening and cooling the subcloud layer. The enhanced cloud downdrafts help explain the layer of relatively cool air above the urban heat island dome shown earlier (Fig. 11a). Furthermore, the Baseline simulation also shows more air masses with warming and drying turbulent entrainment from the free atmosphere into the subcloud layer. Thermodynamically, the enhanced MSE in the subcloud layer (Fig. 11d) is then predominantly maintained by enhanced enthalpy from the surface zone, and partly enhanced by evaporation of the downdrafts and turbulent entrainment. An MSE budget can reveal the proportion of MSE fluxes from each zone, but we refrained to further diagnose the zone contribution fraction because by construction the non-local closure PBL scheme used in our modeling setup limits a detail characterization of the mixing lines within the mixed and subcloud layer.

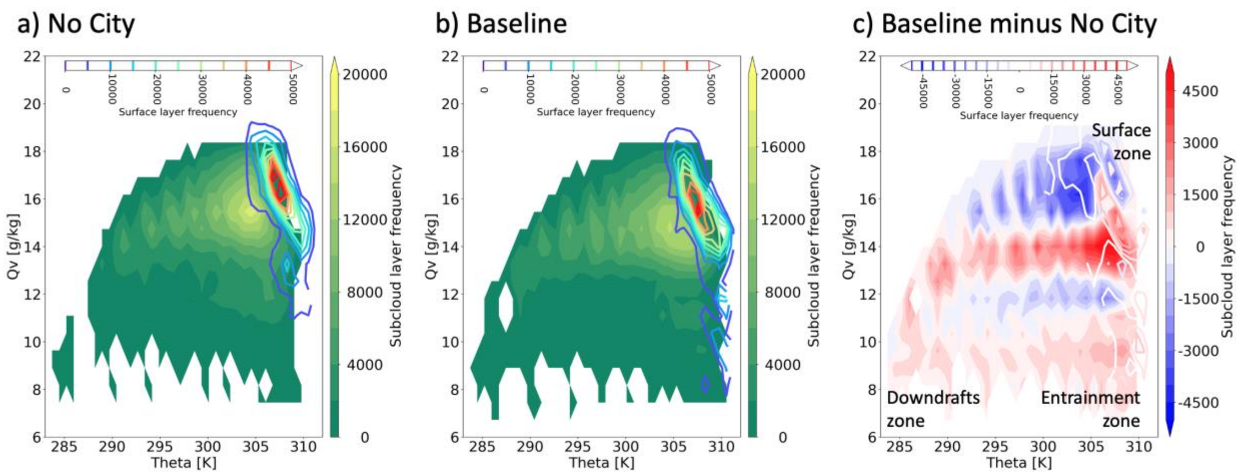

Figure 12. Potential temperature and water vapor mixing ratio (shaded contours) subcloud and (contours) surface layers mixing line distribution analyses over the urban area for (a) No City, (b) Baseline and (c) Baseline minus No City. Only urban grid points in the 12 to 16 LT period were considered.

3.4 SSTs Sensitivity

To test the sensitivity of the urban clouds against regional sources of moisture and mesoscale circulations related to the land-sea contrast, we compared the Baseline with the Biased SST simulations. Fig. 13 shows that the warm SSTs adjustment in the Baseline simulation favors more shallow cumulus clouds. The effect of urbanization, however, is still dominant when compared to the warm SSTs adjustment. Notwithstanding is that the warm SSTs adjustment also increases clouds over the rural areas (not shown). By construction, the warmer SSTs develop a warmer low-level atmosphere, with increased latent heat and water vapor, that in turn, are advected by the predominant southerly and southeasterly flow (Fig. 3). Fig. 14 shows evidence of warming and moistening over the city with some striking asymmetries in relation to the changes in local circulation and the clouds themselves. The enhanced water vapor differences and temperature is related to the more intense MSE signal favoring a thermodynamical pathway for the enhanced clouds with a more unstable lower troposphere, with an enhanced, but weaker relative to the Baseline minus No City, horizontal MFC support. Notably, the urban area shows a low-level cooling and moistening signal in relation to the enhanced clouds, further displaying the role of the urban clouds and subcloud layer processes in the daytime UHI effect.

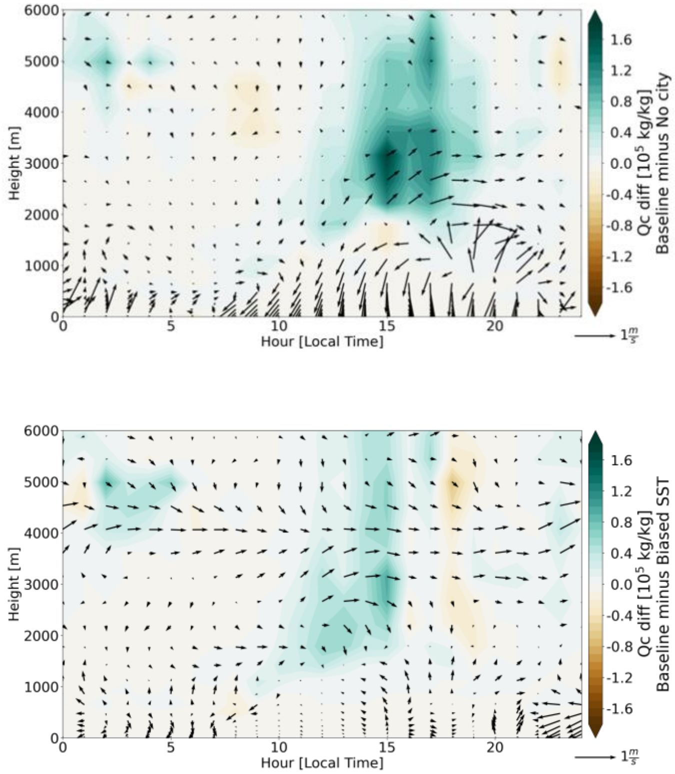

Figure 13. Diurnal-height Cloud mixing ratio and wind vector differences spatially averaged over the urban areas for (top panel) Baseline minus No City and (bottom panel) Baseline minus Biased SST. Vectors in each panel correspond to the horizontal wind, with the north direction pointing upwards). Wind vectors are plotted only every 6 grid point to avoid cluttering.

To better display the impact of the No City and Biased SSTs in the mesoscale circulations, Figs. 15 and 16 show 6-hour averaged diurnal time slices for both interpolated fields at 500 m height and latitude-height slices across the city (Fig. 1). The Baseline minus No City differences show that the urban circulation dome is emphasized as the warm blob collocated with the northerly wind differences. Earlier results showed that this urban circulation dome is favored by the enhanced sensible heat flux, increasing the urban-rural thermal gradient and vertical mixing over the city, and the dynamic frictional drag. Of note is that urbanization imposes anticyclonic and cyclonic differences to the west and east of the city core, with a horizontal scale as large as the urbanization scale and extending vertically as high as 3500 m ASL (Fig. 15; Fan et al. 2017). The urban circulation dome seems to dominate the circulation difference obscuring impacts on the bay- and sea-breeze circulation reported in the literature (Ryu et al. 2016; Shen et al. 2018; Fan et al. 2020; Wang et al. 2023).

The impact of warmer SSTs in the Baseline simulation shows an enhancement of the evening-to-morning land-breeze and a weaker sea-breeze (Fig. 15), which agrees with previous SST sensitivity studies (Ryu et al. 2016; Chen et al. 2011). Characterizing the timing and intensity of the sea breeze in the Houston-Galveston area is complicated by the costal shapes and SST differences with a relatively warmer Galveston Bay compared to the Gulf of Mexico (Salas-Monreal et al. 2018). However, Fig. 16 shows that the weaker sea breeze cell favors the weaker moisture transport near the surface and augment the southerly-southeasterly flow in the return branch of the cell, which help describe the moist difference over the urban area (Fig. 14c). Additionally, the enhanced offshore sensible and latent heat fluxes in the Baseline simulation help develop a deeper and moist MBL (not shown), further enhancing transport of water vapor by the background wind and in the return branch of the sea-breeze.

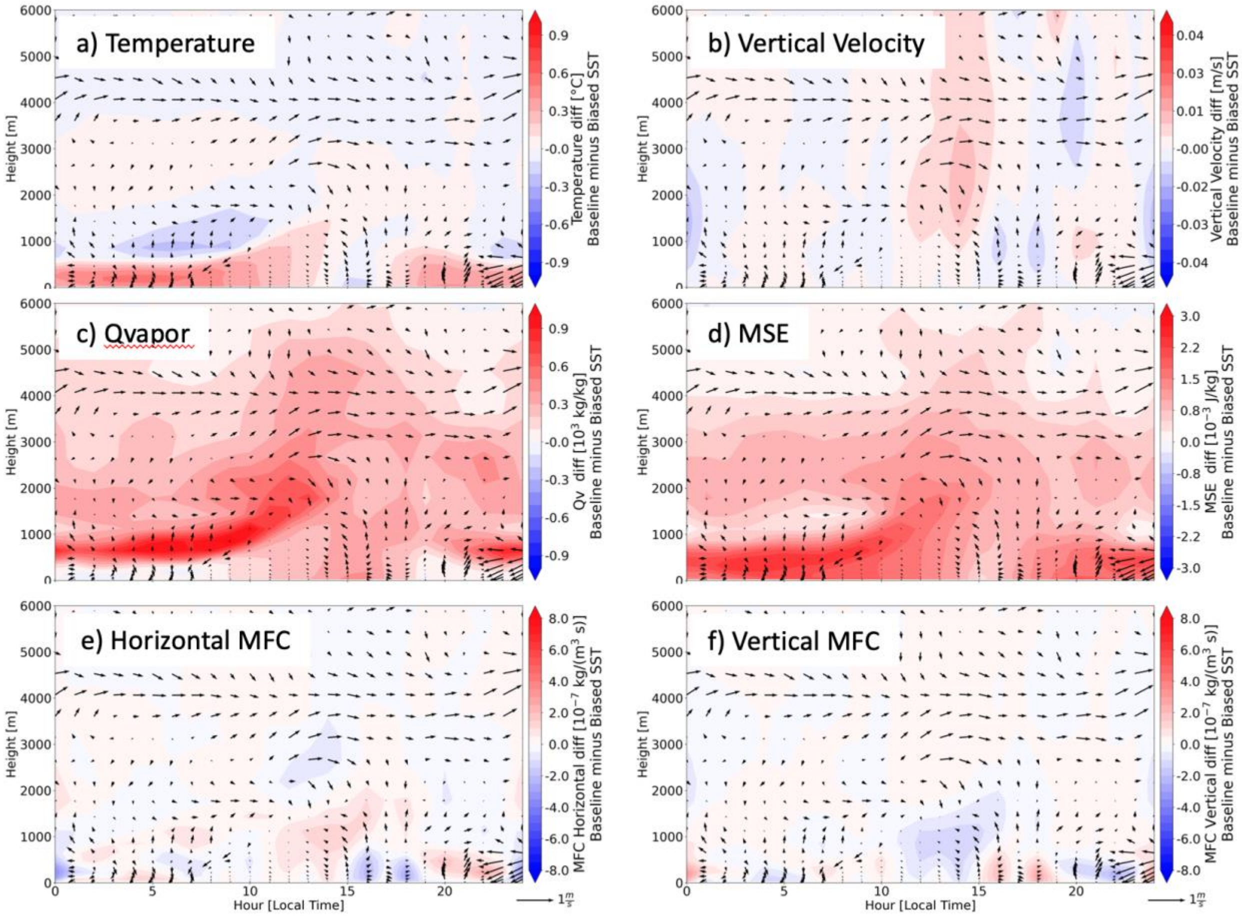

Figure 14. Same as Fig. 11 but for Baseline minus Biased SST scencario differences. Vectors in each panel correspond to the horizontal wind, with the north direction pointing upwards. Wind vectors are plotted only every 6 grid point to avoid cluttering.

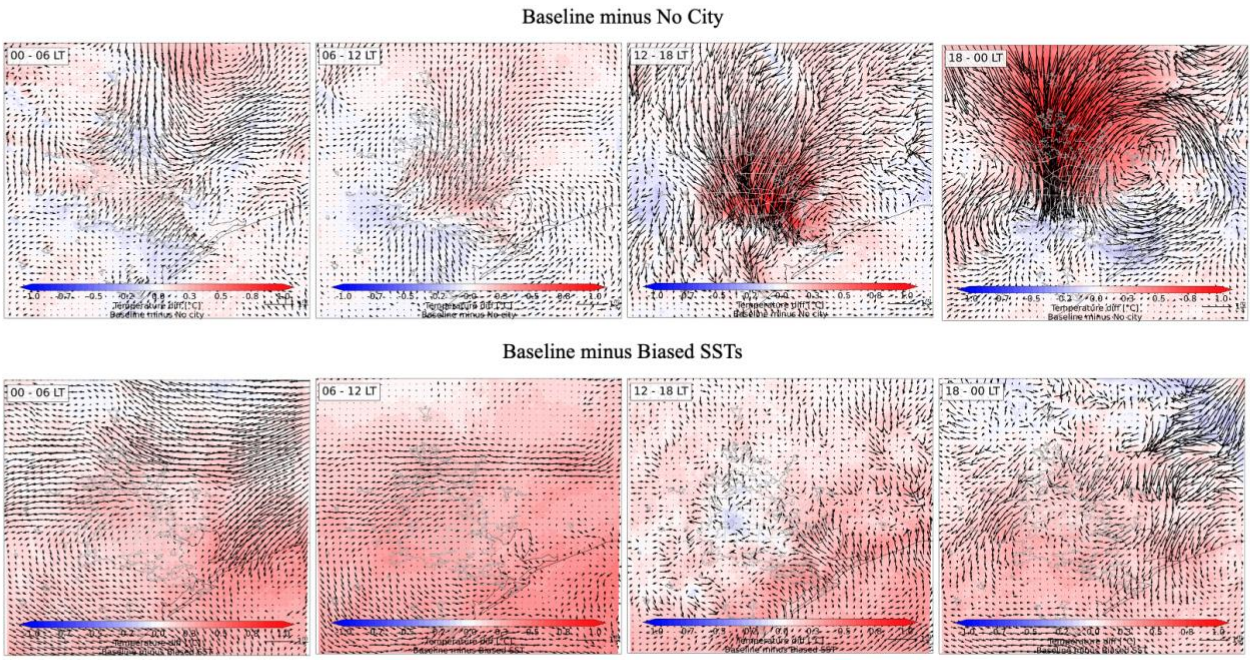

Figure 15. Temperature (contours) and horizontal circulation (vectors) for Baseline minus No City and Baseline minus Biased SSTs differences diurnally averaged over 6-hour time slices (upper left corner in each panel; Local Time). Wind vectors are plotted only every 6 grid point to avoid cluttering. Horizontal analyses show interpolated fields at 500 m height; Dark grey contours indicate urbanization boundaries as of 2010 (Houston-Galveston Area Council, H-GAC; https://www.h-gac.com/Home) and light grey show location of major intraurban highways.

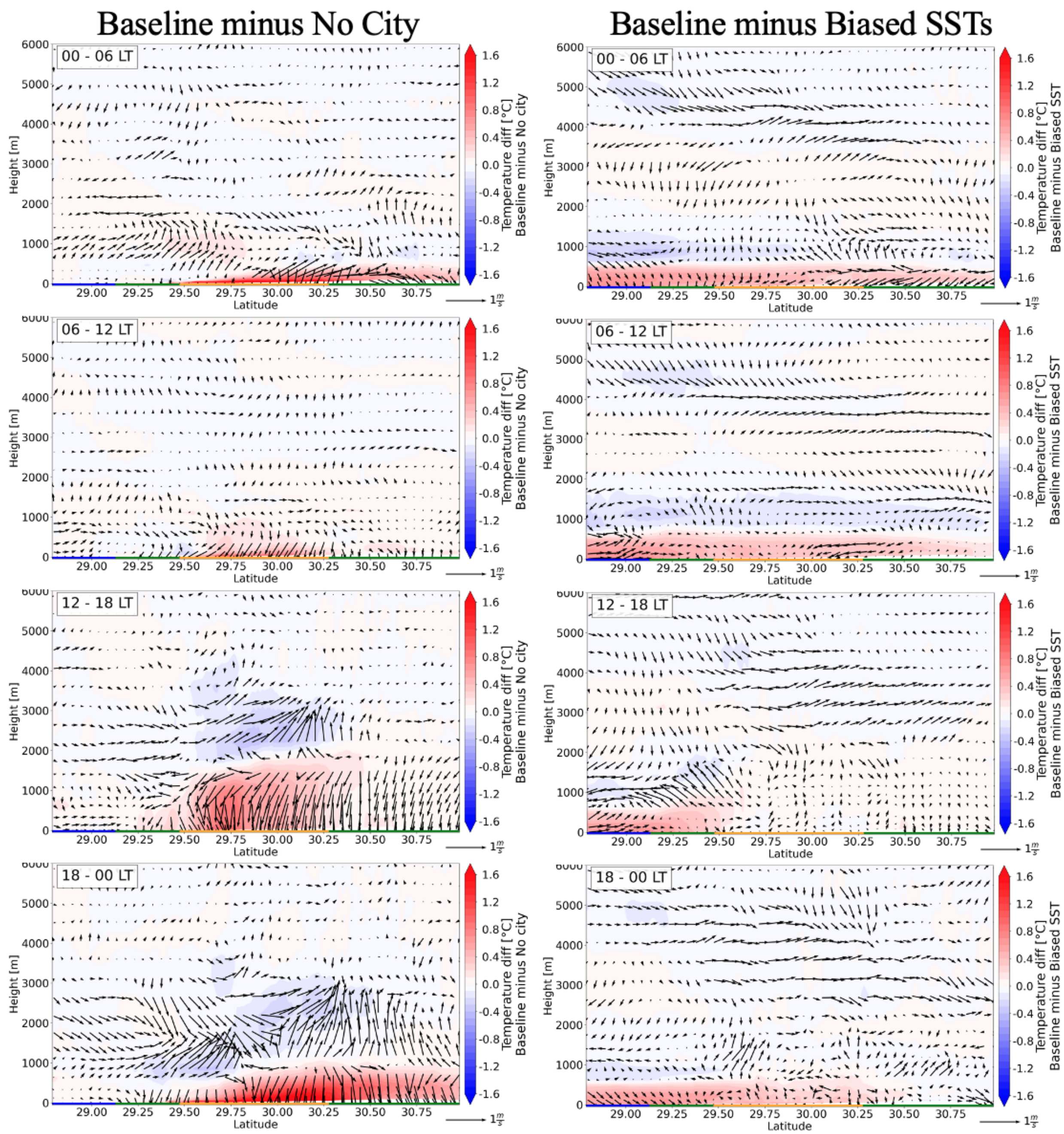

Figure 16. Diurnal evolution (top to bottom) of latitude-height temperature and wind vectors for Baseline minus No City and Baseline minus Bias SST analyses along transect displayed in Fig. 1 with blue, green, and orange lines at the bottom of the panels indicating the location of the water (blue line), rural (green lines), and urban areas (orange line), respectively. Vectors in each panel corresponde to the horizontal wind, with the north direction pointing upwards.

3.5 Heat Index Sensitivity

Here, we examine the role of urbanization, clouds, and SST uncertainties in the Heat Index. Fig. 2 shows that the model has some limitations in simulating the amplitude of the diurnal cycle of the HI over both rural and urban areas, overemphasizing the HI during the nighttime and underemphasizing the HI during the daytime. Although these diurnal biases can be traced to a low performance in simulating the relative humidity, more work is needed to assess the model limitations and sources of uncertainty in stimating the HI. By contrasting the model simulation scenarios, however, we can partly cancel these biases (i.e., linearizing the potential effect of internal feedbacks) and retain the signal related to urbanization, clouds and SST in the diurnal evolution of the HI.

Figure 17 shows the sensitivity of the HI to urbanization and SST adjustments. On the mean, the UHI has a significant influence in increasing the HI mostly during the nighttime and early morning. During high HI times (around 15 LT), however, urbanization is related to weaker HI compared to the rural areas, due to the competing impact of air temperature and relative humidity on the HI. Over the city, the weaker high HI is due partly to the urban dry island effect (Fig. 5), and partly due enhanced clouds and its surface temperature cooling effect (Fig 8), limiting high temperatures in the city (Fig. 6). The sensitivity of the HI to moisture is also shown when contrasting Baseline with the Biased SST simulation. Fig. 17 also shows that the warmer SSTs (~1°C) impact the mean HI with a more intense effect near the coast and over the urbanized areas. During high HI, the HI impact of the warmer SSTs over the urban area is less apparent, likely due to the cloud surface cooling effect balancing the warmer and moist sea breeze (Fig. 14).

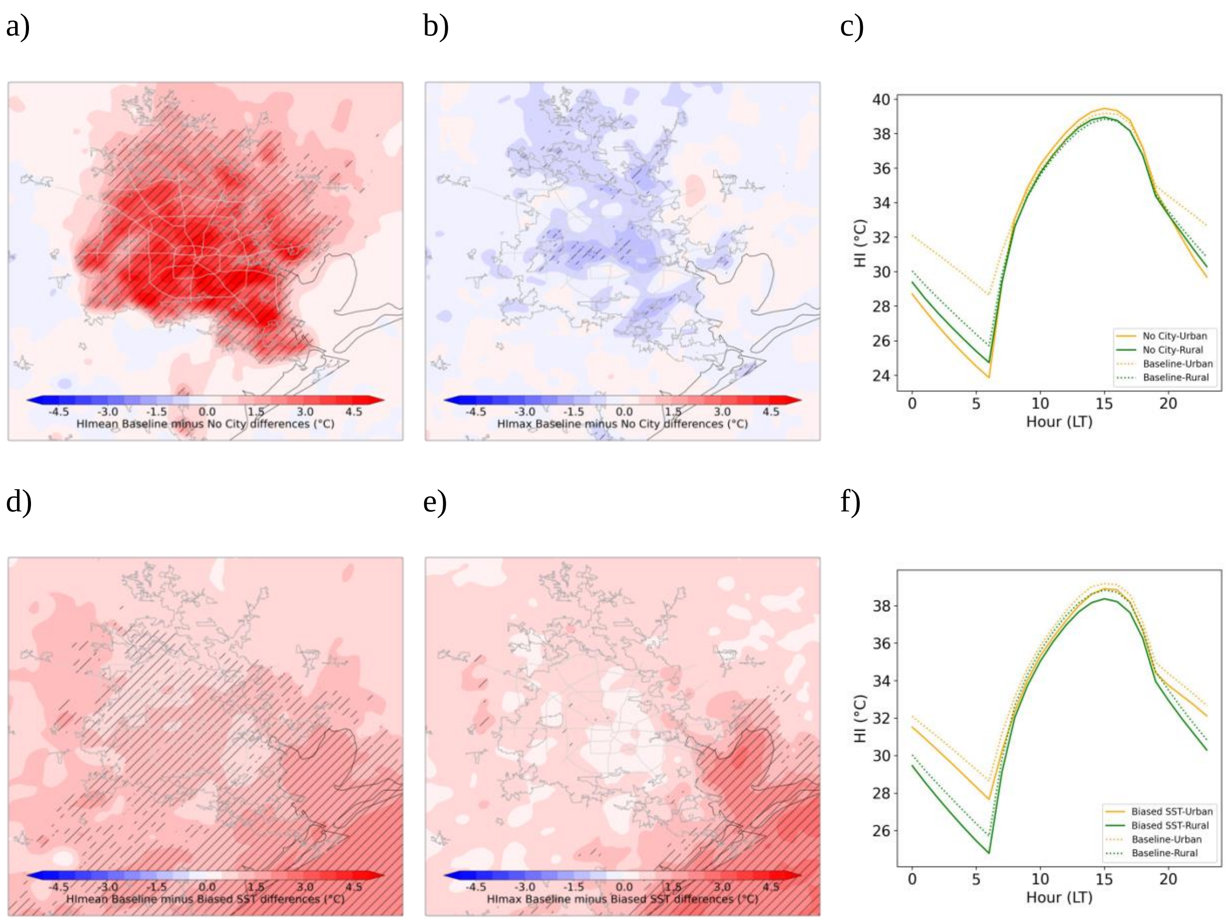

Figure 17. *Mean and diurnal maximum Heat Index (HI) differences for Baseline minus No City (a, b, respectively) and Baseline minus Biased SST (d and e, respectively), with hatched areas indicating that differences are significant with a 95% confidence level; Dark grey contours indicate urbanization boundaries as of 2010 (Houston-Galveston Area Council, H-GAC; https://www.h-gac.com/Home) and light grey show location of major intraurban highways. HI diurnal variability composited by rural and urban areas is also added for (c) Baseline and No City and (f) Baseline and Biased SST.*

4 Discussion and Conclusion

To better understand the effect of urbanization in meteorology, this study developed 900 m grid size simulations using a cloud- and urban-resolving atmospheric model that includes a Building Energy Model coupled with Building Effect Parameterization, over the Houston-Galveston area, between 1-16 August 2020. The study investigates the intricate interplay of clouds in local weather, considering various influencing factors. Several model realizations were developed to isolate the role of the urban environment and to address SST biases in the complex Galveston Bay and Gulf of Mexico coast and its effect in the land-sea circulations known to affect the urban climate (Chen at al. 2011; Ngan et al. 2013; Fan et al. 2020). By excluding local anthropogenic aerosols and their effects, this research provides deeper insights into the relationship between the city and shallow cumulus clouds. These insights contribute to our understanding of the processes modulating excessive heat indicators over urban environments.

Through comprehensive model evaluation using 150 surface station sites, an upper-air wind profiler and a cloud climatology, our analyses reveal that the model simulations perform adequately, but common and well-documented biases remained. In agreement with Ngan et al. (2013), the model overestimates southerly winds by overemphasizing the nighttime low-level jet. Although it is out of the scope of this study, an energy and momentum budget can help elucidate and shed more light on the origin of the existing stronger southerly low-level wind biases. However, the model also simulates a stronger sea breeze, which is somehow consistent with the urban warm surface temperature bias (Fig. 2), and in turn can favor a more intense temperature gradient during the late evening and early morning and maintaining the onshore see-breeze flow much longer. Likewise, the warm nighttime temperature bias could be partly related to the outlined biased low-level southerly winds by favoring more temperature advection from the offshore waters into land and the urban areas. All results and conclusions relying on advection of environmental parameters, including air pollution constituents (Ngan et al. 2013), into or downstream the city need to be assessed with caution. For example, the downstream extend of the UHI impact to the north and northeast of the city may be overemphasized in this model results due to the strong wind bias. Over rural areas, the warm and dry bias could be related to over advection of the UHI and urban dry island effects (Qian et al. 2022; Fig. 4). The bias differences between the urbanized and the No City simulations show that the city is modulating the surface temperature errors, even over the rural areas (UHI advection and UHI dome and related circulations). On the other hand, Fig. 3d shows that the model simulates a weaker sea-breeze at La Porte when compared to the No City scenario. According to Cheng et al. (2011) and Salamanca et al. (2011), the enhanced drag imposed by the city decelerates the flow, which we show reduces the impact of the enhanced thermal driven land-sea circulation due to the warmer city (Fig. 10 and Fig. 15).

It has been suggested that the UHI is more pronounced during the nighttime (Oke 1982), but recent studies have found asymmetries in the time of the maximum diurnal UHI effect, arguing that vegetation type, urban and rural activities (Peng et al. 2012), or clouds (Vo et al. 2023) can affect the time of its maximum. Surface station estimates suggest that during the period of study the UHI was more intense during the afternoon than during the morning, whereas the model suggested the opposite when evaluated at the same surface station locations. This UHI intensity disagreement is common when comparing surface station observations with urban canopy model output (Hu et al. 2019; Venter et al. 2021; Qian et al. 2022). However, estimating the magnitude of the UHI based on surface station observations is a challenging task, including observational uncertainty issues related to limitations of urban stations in following footprint standards (WMO 2008). Moreover, we noted that the magnitude of the UHI is more pronounced farther from the coast, but also varies according to the location of the rural stations relative to the predominant low-level flow, due to outlined advection of UHI downstream from the city. Our results show the typical ground heat flux driving the nighttime UHI, but other meteorological factors became apparent when considering the interaction with mesoscale circulations and clouds. During the afternoon, we speculate that the smaller simulated diurnal UHI can be partly related to overdoing of the urban clouds, limiting temperature highs in the afternoon. During the nighttime, urbanization enhanced uplift water vapor and clouds that slow down nighttime longwave radiation cooling.

Houston-Galveston urbanization favors more shallow cumulus clouds. Our modeling and satellite results support Vo et al. (2023) by showing apparent cloud enhancement due to urbanization. The simulation period for this study coincides with the time of the year when the urbanization cloud patterns are the largest for Gulf Coast coastal cities (Vo et al. 2023). Our results agree with Loughner et al. (2011) and Theeuwes et al. (2019) hypothesis stating that even over urban areas with relatively drier environments, the surface-driven turbulence can sustain longer-lasting clouds compared to the surrounding rural areas. Despite the model uncertainties and biases shown and discussed above, and without considering the role of aerosols, which play a crucial role in the cloud and precipitation invigoration (Fan et al. 2020) in urban environments, our results help understand the mechanistic processes involved in the urban cloud enhancement. Particularly, our simulations confirm the control of the UHI in the clouds by enhanced vertical mixing due to aerodynamical drag and an enhanced sensible heat compared to the surrounding rural areas. In addition, our results also offer a deeper insight on the dynamical and thermodynamical factors interplaying in the cloud enhancement. The city sustains more clouds, with higher cloud heights and deeper shallow cumulus owing to enhanced moist static energy, partly due to enhanced enthalpy by the surface sensible heat and partly due to the enhanced latent heating favored by the enhancement of low-level horizontal moisture flux convergence (Loughner et al. 2011; Fan et al. 2017; Theeuwes et al. 2022; Chiu et al. 2022). We showed that more clouds, in turn, are related to a cooler surface temperature high, when compared to the No City environment and the rural areas surrounding the city. This cooling can further reduce afternoon urban-rural heating contrasts and suppress vertical mixing. However, our mixing line analysis also shows that part of this cooling can also be attributed to evaporative cooling downdraft fluxes. Notwithstanding, enhanced MSE is predominantly maintained by the surface heat fluxes, with a minor role from the warm air entrainment fluxes. All these mechanisms also help understand the precipitation enhancement associated with urbanization (SFig. 4; Ryu et al. 2016; Zhu et al., 2016; Lorenz et al. 2019; Madeline et al. 2021; Fan et al. 2020, Chiu et al. 2022; Wang et al. 2023) and aerosol-cloud interaction and air pollution impacts (Loughner et al. 2011; Seigel 2014; Fan et al. 2020; Zhong et al. 2015, 2017; Caicedo et al. 2019), which are ongoing observational and modeling research foci in the area (Jensen et al. 2022).

For the first time, our results suggest that the enhanced drag, sensible heat, and vertical mixing related to urbanization act as an obstacle to the prevailing flow, favoring urban circulation dome patterns with a horizontal scale of influence as large as the urban area (Fan et al. 2017). Previous studies have suggested that the UHI circulation can strengthen the sea breeze circulation, which favors moisture flux convergence and cooler airflow into the urban environment (Ryu et al. 2016; Zhong et al. 2017; Shen et al. 2018; Fan et al. 2020). However, our results show that dynamical fictional drag due to urbanization slows down the low-level flow with a scale of influence that appears to weaken the thermal-driven bay- and sea-breezes influencing the city. It is possible that deceleration owning the urban-dynamical drag effect becomes less prominent, and the urban land effect on the sea breeze circulation can become more evident, during weaker or different south-southwesterly background flow regimes (Chen et al. 2011; Ngan et al. 2013; Wang et al. 2022).

Urbanization increases the mean HI, but at the time of high HI, urbanization shows less intense HI, due to the cloud pathway as a cooling mechanism. Additionally, the model sensitivities to SSTs revealed that the coastal environment can modulate the UHI intensity, with warmer SSTs producing cooler urban surface temperature highs due to a similar enhanced shallow cumulus cloud pathway, despite the weaker but warmer and moist sea-breeze. Near the coast, the effect of the warmer and more humid environment advected by the sea-breeze due to the warmer SSTs appears to have a net intensification of the urban HI, whereas the high HI does not show significant sensitivity, likely due to the competing factors between the surface temperature and relative humidity. These results offer new insight and complements other studies focusing on urbanization and related modulation of the sea breeze as driving mechanisms of the urban heat stress and transport problems in cities near large surface water bodies (Shen et al. 2018; Caicedo et al. 2019; Wang et al. 2023).

Modeling work aiming to assess the impact of heat adaptation and mitigation strategies need to assess the tradeoffs in the UHI circulations and clouds pathways relationships. Most mesoscale urban heat mitigation modeling studies suggest different cooling strategies influencing city scale net cooling effects ranging from ~0.1 to a few degrees °C, depending on the intensity of the implementation (Krayenhoff et al. 2021), but often assume that model biases and other errors are somehow steady under different model conditions and disregard the effect of model errors on relevant physical process. Hence, the impact of cooling strategies can be overwhelmed by uncertainties in SST fields (i.e., those related to observations and data assimilation uncertainties), or by the accuracy of the simulated clouds and precipitation, which is typically an important source of uncertainty in the model.

Acknowledgement: This work was funded by NOAA-Climate Program Office Extreme Heat Risk Initiative grant number NA21OAR4310149. City of Houston - Mayor's Office *of Resilience and* Sustainability *and National Weather Service Forecast Office (Timothy Cady), Houston-*

Galveston, TX for their support in this study. High-performance computing was partially provided the University of Nevada's Office of Information Technology, Research & Innovation, and the Nevada Governor's Office for Economic Development. We extend out thanks to Drs. Zonato Andrea and Alberto Martilli for their insight in numerical diffusion configuration issues in earlier versions of our model configurations.

Open Research

All the observational data needed to develop this study is readily available online. Model configuration needed to replicate the simulations are described in the text. Readers can reach out the correspondent author for details and model output availability and postprocessing software (Python) used in the analyses.

References

Ancell, B. C., A. Bogusz, M. J. Lauridsen, and C. J. Nauert (2018), Seeding Chaos: The Dire Consequences of Numerical Noise in NWP Perturbation Experiments. *Bull. Amer. Meteor. Soc.*, 99, 615–628, https://doi.org/10.1175/BAMS-D-17-0129.1.

Blackadar, A. K. (1957), Boundary layer wind maxima and their significance for the growth of nocturnal inversions. *Bull. Amer. Meteor. Soc.*, 38, 283– 290.

Brenguier, J., Pawlowska, H., Schüller, L., Preusker, R., Fischer, J., and Fouquart, Y. (2000), Radiative Properties of Boundary Layer Clouds: Droplet Effective Radius versus Number Concentration, *Journal of the Atmospheric Sciences*, 57(6), 803-821. https://journals.ametsoc.org/view/journals/atsc/57/6/1520-0469_2000_057_0803_rpoblc_2.0.co_2.xml

Bouali, M., and A. Ignatov (2014), Adaptive Reduction of Striping for Improved Sea Surface Temperature Imagery from Suomi National Polar-Orbiting Partnership (S-NPP) Visible Infrared

Imaging Radiometer Suite (VIIRS). *J. Atmos. Oceanic Technol.*, 31, 150–163, https://doi.org/10.1175/JTECH-D-13-00035.1.

Brousse Oscar, Alberto Martilli, Michael Foley, Gerald Mills, Benjamin Bechtel (2016), WUDAPT, an efficient land use producing data tool for mesoscale models? Integration of urban LCZ in WRF over Madrid, *Urban Climate*, 17, 116-134, https://doi.org/10.1016/j.uclim.2016.04.001.

Cady, T. J., Rahn, D. A., Brunsell, N. A., & Lyles, W. (2020), Conversion of Abandoned Property to Green Space as a Strategy to Mitigate the UHI Investigated with Numerical Simulations, *J. Appl. Meteor. Climatol.*, 59(11), 1827-1843. https://doi.org/10.1175/JAMC-D-20-0093.1

Caicedo, V., et al. (2019), Bay breeze and sea breeze circulation impacts on the planetary boundary layer and air quality from an observed and modeled DISCOVER-AQ TX case study. *Journal of Geophysical Research: Atmospheres*, 124, 7359–7378. https://doi.org/10.1029/2019JD030523

Chen F., Miao S., Tewari M., Bao J.W., Kusaka H (2011), A numerical study of interactions between surface forcing and sea breeze circulations and their effects on stagnation in the greater Houston area. *J. Geophys. Res. Atmos.*;116:1–19. doi: 10.1029/2010JD015533.

Ching, J., and Coauthors (2009), National Urban Database and Access Portal Tool. *Bull. Amer. Meteor. Soc.*, 90, 1157–1168, https://doi.org/10.1175/2009BAMS2675.1.

Ching, J., Mills, G., Bechtel, B., See, L., Feddema, J., Wang, X., … Theeuwes, N. (2018), WUDAPT: An Urban Weather, Climate, and Environmental Modeling Infrastructure for the Anthropocene. *Bull. Amer. Meteor. Soc.*, 99(9), 1907–1924. https://doi.org/10.1175/BAMS-D-16-0236.1

Chiu C.T.F., Kai Wang, Athanasios Paschalis, Tohid Erfani, Nadav Peleg, Simone Fatichi, Natalie Theeuwes, Gabriele Manoli (2022), An analytical approximation of urban heat and dry islands and their impact on convection triggering, *Urban Climate*, 46, https://doi.org/10.1016/j.uclim.2022.101346.

Crosman, Erik T. and Horel, John D. (2012), Idealized Large-Eddy Simulations of Sea and Lake Breezes: Sensitivity to Lake Diameter, Heat Flux and Stability, *Boundary-Layer Meteorology*, 144(3), 309–328, https://doi.org/10.1007/s10546-012-9721-x

Demuzere M, Kittner J, Bechtel B. (2021), LCZ Generator: A Web Application to Create Local Climate Zone Maps. *Front Environ Sci*.;9. doi:10.3389/fenvs.2021.637455.

Demuzere, M., Kittner, J., Martilli, A., Mills, G., Moede, C., Stewart, I. D., van Vliet, J., and Bechtel, B. (2022), A global map of Local Climate Zones to support earth system modelling and urban scale environmental science, *Earth Syst. Sci. Data* 14(8) 3835-3873. DOI: 10.5194/essd-14-3835-2022.

Doan, Q., S. Kobayashi, H. Kusaka, F. Chen, C. He, and D. Niyogi (2023), Tracking Urban Footprint on Extreme Precipitation in an African Megacity. *J. Appl. Meteor. Climatol.*, 62, 209–226, https://doi.org/10.1175/JAMC-D-22-0048.1.

Ebi, K. L., Capon, A., Berry, P., Broderick, C., de Dear, R., Havenith, G., ... & Jay, O. (2021), Hot weather and heat extremes: health risks. *The Lancet*, 398(10301), 698-708.

Fan, J., Zhang, Y., Li, Z., Hu, J., and Rosenfeld, D. (2020), Urbanization-induced land and aerosol impacts on sea-breeze circulation and convective precipitation, *Atmos. Chem. Phys.*, 20, 14163–14182, https://doi.org/10.5194/acp-20-14163-2020.

Fan, Y. F., Y. G. Li, A. Bejan, Y. Wang, and X. Y. Yang (2017), Horizontal extent of the urban heat dome flow. *Scientific Reports*, 7, 11681, https://doi.org/10.1038/s41598-017-09917-4.

Fischer, E., Schär, C. (2010), Consistent geographical patterns of changes in high-impact European heatwaves. *Nature Geosci*, 3, 398–403, https://doi.org/10.1038/ngeo866

Guo Y, Gasparrini A, Li S, Sera F, Vicedo-Cabrera AM, de Sousa Zanotti Stagliorio Coelho M, et al. (2018), Quantifying excess deaths related to heatwaves under climate change scenarios: A multicountry time series modelling study. *PLoS Med* 15(7): e1002629.

Hawbecker, P., and J. C. Knievel (2022), Simulating the Chesapeake Bay Breeze: Sensitivities to Water Surface Temperature. *J. Appl. Meteor. Climatol.*, 61, 1595–1611, https://doi.org/10.1175/JAMC-D-22-0002.1.

Hendricks, E. A., Knievel, J. C., & Wang, Y. (2020), Addition of Multilayer Urban Canopy Models to a Nonlocal Planetary Boundary Layer Parameterization and Evaluation Using Ideal and Real Cases, *J.*

Appl. Meteor. Climatol., 59(8), 1369-1392, https://journals.ametsoc.org/view/journals/apme/59/8/jamcD190142.x

Houston Climate Action Plan (2020), http://greenhoustontx.gov/climateactionplan/

Hu, Y. H., M. T. Hou, G. S. Jia, C. L. Zhao, X. J. Zhen, and Y. H. Xu (2019), Comparison of surface and canopy urban heat islands within megacities of eastern China. *ISPRS Journal of Photogrammetry and Remote Sensing*, 156, 160−168, https://doi.org/10.1016/j.isprsjprs.2019.08.012.

Jensen, M. P., Flynn, J. H., Judd, L. M., Kollias, P., Kuang, C., Mcfarquhar, G., Nadkarni, R., Powers, H., and Sullivan, J. (2022), A succession of cloud, precipitation, aerosol, and air quality field experiments in the coastal urban environment, *Bull. Amer. Meteor. Soc.*, 103(2), 103-105. https://journals.ametsoc.org/view/journals/bams/103/2/BAMS-D-21-0104.1.xml

Jin, L., Schubert, S., Fenner, D. et al. (2021), Integration of a Building Energy Model in an Urban Climate Model and its Application. Boundary-Layer Meteorol, 178, 249–281. https://doi.org/10.1007/s10546-020-00569-y

Knievel, J. C., Bryan, G. H., & Hacker, J. P. (2007), Explicit Numerical Diffusion in the WRF Model, *Monthly Weather Review*, 135(11), 3808-3824. https://journals.ametsoc.org/view/journals/mwre/135/11/2007mwr2100

Krayenhoff, Eric and Broadbent, Ashley & Zhao, Lei & Georgescu, Matei & Middel, Ariane & Voogt, James and Martilli, Alberto & Sailor, David & Erell, Evyatar. (2021), Cooling hot cities: A systematic and critical review of the numerical modelling literature. *Environmental Research Letters*, 16, 10.1088/1748-9326/abdcf1.

Lorenz, J. M., Kronenberg, R., Bernhofer, C., & Niyogi, D. (2019), Urban rainfall modification: Observational climatology over Berlin, Germany. *Journal of Geophysical Research: Atmospheres*, 124, 731–746. https://doi.org/10.1029/2018JD028858

Loughner, C. P., D. J. Allen, K. E. Pickering, R. R. Dickerson, D.-L. Zhang, and Y.-X. Shou (2011), Impact of the Chesapeake Bay breeze and fair-weather cumulus clouds on pollutant transport and transformation. *Atmos. Environ.*, 24, 4060–4072.

Madeline D. Statkewicz, Robert Talbot, Bernhard Rappenglueck (2021), Changes in precipitation patterns in Houston, Texas, *Environmental Advances*, 5, 100073, ISSN 2666-7657, https://doi.org/10.1016/j.envadv.2021.100073.

Morris, C. J. G., Simmonds, I., Plummer, N. (2001), Quantification of the Influences of Wind and Cloud on the Nocturnal Urban Heat Island of a Large City. *Journal of Applied Meteorology,* 40(2), 169-18.

Ngan, F., H. Kim, P. Lee, K. Al-Wali, and B. Dornblaser (2013), A Study of Nocturnal Surface Wind Speed Overprediction by the WRF-ARW Model in Southeastern Texas. *J. Appl. Meteor. Climatol.*, 52, 2638–2653, https://doi.org/10.1175/JAMC-D-13-060.1.

Oke, T. R. (1982), The energetic basis of the urban heat island. *Q. J. R. Meteorolog. Soc.* 108, 1–24.

Peng, S. et al. (2012), Surface urban heat island across 419 global big cities. *Environ. Sci. Technol.* 46, 696–703. https://doi.org/10.1021/es2030438

Pu, B., and R. E. Dickinson (2014), Diurnal Spatial Variability of Great Plains Summer Precipitation Related to the Dynamics of the Low-Level Jet. *J. Atmos. Sci.*, 71, 1807–1817, https://doi.org/10.1175/JAS-D-13-0243.1.

Qian Y, Chakraborty TC, Li J, Li D, He C, Sarangi C, Chen F, Yang X, Leung LR. (2022), Urbanization Impact on Regional Climate and Extreme Weather: Current Understanding, Uncertainties, and Future Research Directions. *Adv Atmos Sci.* 2022;39(6):819-860. doi: 10.1007/s00376-021-1371-9.

Resilient Houston, (2020). https://www.houstontx.gov/mayor/Resilient-Houston-20200518-single-page.pdf

Rosenzweig, C., et al. (2014), Enhancing Climate Resilience at NASA Centers: A Collaboration between Science and Stewardship, *Bull. Amer. Meteor. Soc.*, 95(9), 1351-1363, https://journals.ametsoc.org/view/journals/bams/95/9/bams-d-12-00169.1.xml

Rothfusz, L. P. (1990), The heat index “equation” (or, more than you ever wanted to know about heat index). NWS Tech. Attachment SR 90-23, 2 pp.

Ryu, Y., J. A. Smith, E. Bou-Zeid, and M. L. Baeck (2016), The Influence of Land Surface Heterogeneities on Heavy Convective Rainfall in the Baltimore–Washington Metropolitan Area. *Mon. Wea. Rev.*, 144, 553–573, https://doi.org/10.1175/MWR-D-15-0192.1.

Salamanca, F., A. Martilli, M. Tewari, and F. Chen (2011), A Study of the Urban Boundary Layer Using Different Urban Parameterizations and High-Resolution Urban Canopy Parameters with WRF. *J. Appl. Meteor. Climatol.*, 50, 1107–1128, https://doi.org/10.1175/2010JAMC2538.1.

Salas-Monreal D., Ayal Anis, David Alberto Salas-de-Leon (2018), Galveston Bay dynamics under different wind conditions, *Oceanologia*, 232-243, https://doi.org/10.1016/j.oceano.2017.10.005.

Schubert S, Grossman-Clarke S, Martilli A. (2012), A double-canyon radiation scheme for multi-layer urban canopy models. *Boundary-Layer Meteorol*, 145(3):439–468

Seigel, R. B. (2014), Shallow Cumulus Mixing and Subcloud-Layer Responses to Variations in Aerosol Loading. *J. Atmos. Sci.*, 71, 2581–2603, https://doi.org/10.1175/JAS-D-13-0352.1.

Shen, L. D., J. N. Sun, and R. M. Yuan (2018), Idealized large eddy simulation study of interaction between urban heat island and sea breeze circulations. *Atmospheric Research*, 214, 338−347, https://doi.org/10.1016/j.atmosres.2018.08.010.

Simolo, C., Brunetti, M., Maugeri, M., and Nanni, T. (2011), Evolution of extreme temperatures in a warming climate, *Geophys. Res. Lett.*, 38, L16701, doi:10.1029/2011GL048437.

Skamarock, W. C., and Coauthors (2008), A description of the Advanced Research WRF version 3. *NCAR Tech. Note* NCAR/TN-475+STR, 113 pp., doi:10.5065/D68S4MVH.

Theeuwes N. E., I. A. Boutle, P. A. Clark, S. Grimmond (2021), Understanding London’s summertime cloud cover. *Q. J. R. Meteorol. Soc*. 148(742), 454–465. https://doi.org/10.1002/qj.4214

Theeuwes, N.E., Barlow, J.F., Teuling, A.J. *et al.* (2019), Persistent cloud cover over mega-cities linked to surface heat release. *npj Clim Atmos Sci* **2**, 15. https://doi.org/10.1038/s41612-019-0072-x

Trenberth, K., Fasullo, J. & Shepherd, T. (2015), Attribution of climate extreme events. *Nature Clim Change* 5, 725–730 https://doi.org/10.1038/nclimate2657

USGCRP (2018), Impacts, Risks, and Adaptation in the United States: Fourth National Climate Assessment, *Volume II* [Reidmiller, D.R., C.W. Avery, D.R. Easterling, K.E. Kunkel, K.L.M. Lewis, T.K. Maycock, and B.C. Stewart (eds.)]. U.S. Global Change Research Program, Washington, DC, USA, 1515 pp. doi: 10.7930/NCA4.2018.

Venter, Z. S., T. Chakraborty, and X. Lee (2021), Crowdsourced air temperatures contrast satellite measures of the urban heat island and its mechanisms. *Science Advances*, 7, eabb9569, https://doi.org/10.1126/sciadv.abb9569.

Vo, Trang Thuy & Hu, Leiqiu & Xue, Lulin & Li, Qi & Chen, Sisi (2023), Urban effects on local cloud patterns. *Proceedings of the National Academy of Sciences of the United States of America*. 120. e2216765120. 10.1073/pnas.2216765120.

Wang Jiali, Yun Qian, William Pringle, T.C. Chakraborty, Robert Hetland, Zhao Yang, Pengfei Xue (2023), Contrasting effects of lake breeze and urbanization on heat stress in Chicago metropolitan area, *Urban Climate*, 48, https://doi.org/10.1016/j.uclim.2023.101429.

Wang, D., Jensen, M. P., Taylor, D., Kowalski, G., Hogan, M., Wittemann, B. M., et al. (2022), Linking synoptic patterns to cloud properties and local circulations over southeastern Texas. *Journal of Geophysical Research: Atmospheres*, 127, e2021JD035920. https://doi.org/10.1029/2021JD035920

Williams, A. P., Schwartz, R. E., Iacobellis, S., Seager, R., Cook, B. I., Still, C. J., Husak, G. and Michaelsen, J. (2015), Urbanization causes increased cloud base height and decreased fog in coastal Southern California. *Geophys. Res. Lett.*, 42: 1527– 1536. doi: 10.1002/2015GL063266.

Wilson AM, Jetz W (2016), Remotely Sensed High-Resolution Global Cloud Dynamics for Predicting Ecosystem and Biodiversity Distributions. *PLoS Biol* 14(3): e1002415. doi:10.1371/journal. pbio.1002415" Data available on-line at http://www.earthenv.org/.

WMO (2008), Guide to Meteorological Instruments and Methods of Observation. World Meteorological Organization.

Zhong, S., Qian, Y., Zhao, C., Leung, R., and Yang, X. Q. (2015), A case study of urbanization impact on summer precipitation in the Greater Beijing Metropolitan Area: Urban heat island versus aerosol effects, *J. Geophys. Res.-Atmos.*, 120, 10903–10914, https://doi.org/10.1002/2015jd023753.

Zhong, S., Qian, Y., Zhao, C., Leung, R., Wang, H., Yang, B., Fan, J., Yan, H., Yang, X.-Q., and Liu, D. (2017), Urbanization-induced urban heat island and aerosol effects on climate extremes in the Yangtze River Delta region of China, *Atmos. Chem. Phys.*, 17, 5439–5457, https://doi.org/10.5194/acp-17-5439-2017.

Zhu, X., Ni, G., Cong, Z., Sun, T., and Li, D. (2016), Impacts of surface heterogeneity on dry planetary boundary layers in an urban-rural setting, *J. Geophys. Res. Atmos.*, 121, 12,164– 12,179, doi:10.1002/2016JD024982.

Zonato, A., Martilli, A., Gutierrez, E., Chen, F., He, C., Barlage, M., et al. (2021), Exploring the effects of rooftop mitigation strategies on urban temperatures and energy consumption. *Journal of Geophysical Research: Atmospheres*, 126, e2021JD035002. https://doi.org/10.1029/2021JD035002

5 Supplemental Material

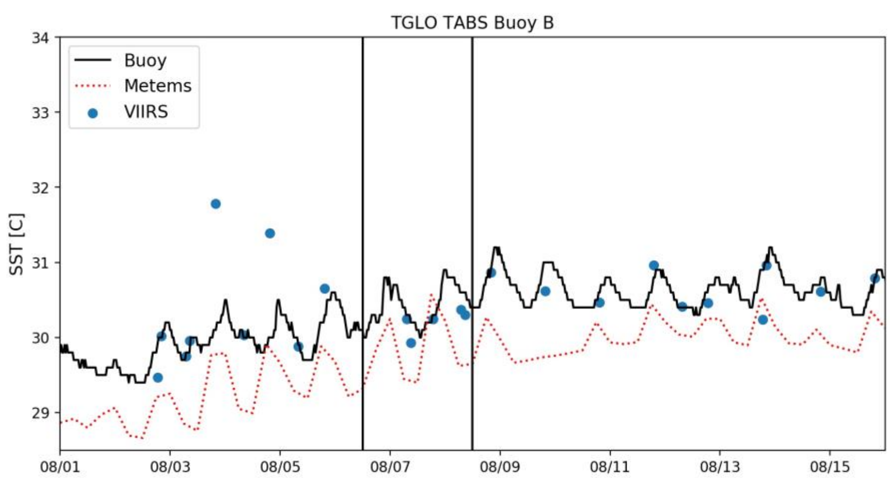

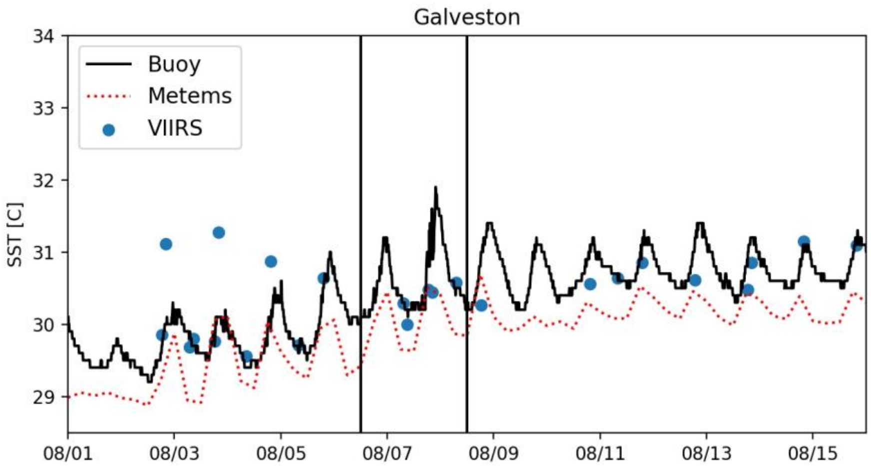

SFigure 1. (Top panel) TGLO TABS Buoy B and (bottom panel) Galveston hourly buoy SST, twice a day remotely sensed data (NOAA-SNPP VIIRS SST) and untreated-biased SST (after preprocessed by WRF). Date (MM/DD) range for the first half of August 2020.

a) Surface temperature RMSE

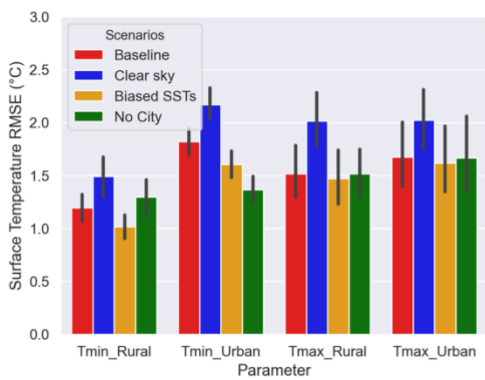

b) Relative humidity RMSE

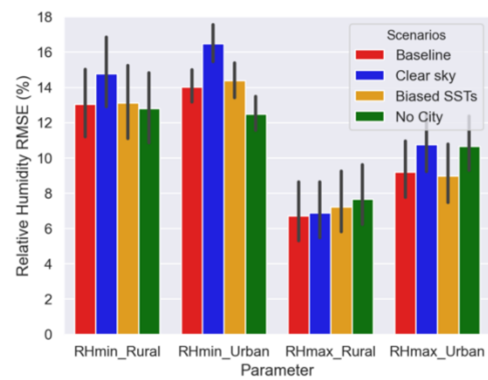

c) Surface temperature Pearson correlation

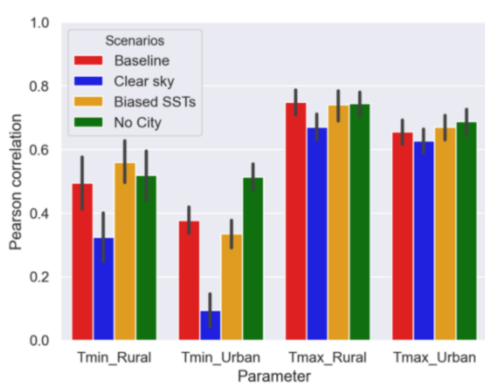

d) Relative humidity Pearson correlation

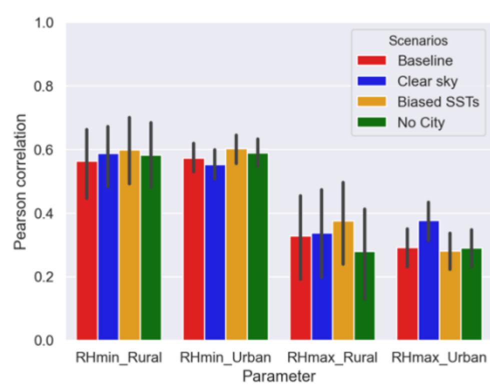

SFigure 2. Simulated RMSE and Pearson correlation for evaluated at surface station sites for different scenarios (Table 2) for (a, c) daily for surface temperature low and high (Tmin, Tmax), (b, d) relative humidity maximum and minimum (RHmax, RHmin), and corresponding bias distribution for all examined surface station sites as categorized as Urban or Rural according to MODIS/WUDAPTv2 land use/land cover types. Evaluation period is 1-16 August 2020. Analysis constrained to non-rainy periods as described in the text.

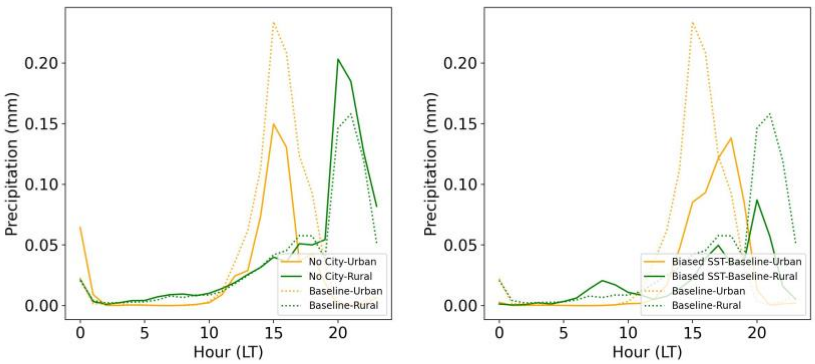

SFigure 4. Spatially averaged diurnal precipitation in the urban and rural areas for (left panel) Baseline and No City and (right panel) Baseline and Biased-SST scenarios.